energies

MDPI

Article

Sedimentary and Diagenetic Features and Their Impacts on Microbial Carbonate Reservoirs in the Fourth Member of the Middle Triassic Leikoupo Formation, Western Sichuan Basin, China

Yuanchong Wang [1], Weimin Jiang [1], Hangyu Liu [1], Bo Liu [1,*], Haofu Zheng [2], Xiaobo Song [3], Qiongxian Wang [3], Wenkai Wang [3] and Yong Li [3]

1 School of Earth and Space Sciences, Peking University, Beijing 100871, China; wangyuanchong@pku.edu.cn (Y.W.); 1601110591@pku.edu.cn (W.J.); 1801110626@pku.edu.cn (H.L.)
2 College of River and Ocean Engineering, Chongqing Jiaotong University, Chongqing 400074, China; zhenghaofu@cqjtu.edu.cn
3 Research Institute of Petroleum Exploration and Development, Southwest Petroleum Branch, SINOPEC, Chengdu 610041, China; sxbtop@163.com (X.S.); Wqxtop@163.com (Q.W.); wwk-dyx@163.com (W.W.); lycup0214@163.com (Y.L.)
* Correspondence: bobliu@pku.edu.cn

Received: 6 March 2020; Accepted: 28 April 2020; Published: 6 May 2020

Abstract: In recent years, the discovery of two gas fields in the fourth member of the Leikoupo Formation in the Western Sichuan Basin of SW China confirmed the exploration potential of microbial carbonates. The aim of the present study is to clarify the formation mechanism of the microbial reservoirs in the Leikoupo Formation. For this purpose, lithofacies, depositional environments, and diagenesis analyses were performed in samples collected from cores of 12 wells. The climate of study area was arid during Anisian time, and the water body was restricted. In such a climate, an evaporitic environment was developed, where ten types of lithofacies, dominated by microbial carbonates and gypsum rocks, were recognized. Thrombolites and stromatolites are the main high-quality reservoirs rock types in the fourth member of the Leikoupo Formation in the Western Sichuan Basin of SW China, which developed as microbial mounds, with reservoir space of microbial inter-clot pores, intra-clot pores, fenestral pores, inter-crystalline pores, and cracks. The microbial inter-clot pores are the main reservoir space, formed by trapping and binding of marls by benthic microbial communities. These pores were partially filled with evaporites because of the arid climate, which were subsequently dissolved (mainly gypsum) in the syn-depositional period, thus greatly improving the quality of reservoirs. Although some pores were occluded by multi-stage cements during the burial stage, major pores were well preserved own to the early dolomitization, rapid burial of the Leikoupo Formation, and early charging of hydrocarbon. The early dolomitization enhanced the anti-compaction ability of microbial carbonates during the burial stage. Rapid burial of the Leikoupo succession slowed down early cementation, and it also accelerated the maturation and expulsion process source rock to promote early charging of hydrocarbon in pores, which created a closed system, inhibiting strong burial cementation.

Keywords: sedimentation; diagenesis; microbial carbonates; reservoir formation; the Middle Triassic Leikoupo Formation; the Western Sichuan Basin of SW China

1. Introduction

Microbialites are organosedimentary $CaCO_3$ deposits, which are formed by the trapping and binding of detrital sediments of the benthic microbial communities [1,2]. Microbial carbonates, one common type of microbialites, are classified into stromatolite, thrombolite, dendrolite, and leiolite [3]. Microbial carbonates are considered the most ancient biological record on Earth, beginning around 3.5 bya [4], while in modern times, microbial carbonates are nearly extinct in normal marine environments but continue to form in extreme environments with high salinity, high alkalinity, high temperature, and low temperature, such as Shark Bay [5,6], Bahamas [7–9], High-altitude Lakes in Argentina [10], and Ruidera [11].

Microbial carbonates have a wide distribution in geological history and have been globally developed since the Archean [12,13]. Chronologically, microbial carbonate rocks were mostly developed during turning points in geological history, such as the Ordovician-Silurian [14] and the Permian-Triassic [15,16]. Regionally, microbial carbonates developed in Armenia [17], Iran [18], Hungary [19], Northern Italy [20], Turkey [21], Sichuan [22,23], and Xinjiang [24,25]. There are also much researches on modern microbial carbonate rocks, such as the pyramidal stromatolites and small minaret stromatolites in the Antarctic [26], the coarse-grained stromatolite in Bahama [27], and the fine-grained stromatolite in Australia [28]. In addition, in recent years, microbial carbonates have shown a great economic potential, since reservoirs related to them have been found in multiple oil and gas fields around the world [15,16,29–34]. Thrombolites and stromatolites have more than 3.5×10^8 t of oil reserves in the Salt Basin of Oman [31]. The Upper Jurassic thrombolite reserves 6.8×10^9 t oil potential in the Santos Basin of Brazil [32]. The Smackover Formation in Alabama has reserves of 2.49×10^7 t of oil and 1.4×10^8 m^3 of gas in thrombolite [30,33]. The Upper Permian shows a great reservoir potential of thrombolite and stromatolite [15]. The Wumishan Formation in Renqiu oil field has reserves of 9.6×10^8 t of oil in stromatolites and thrombolites [29]. The Dengying Formation in Sichuan Basin has reserves of 100 billion m^3 of gas in thrombolite, stromatolite, and peloid dolomite [16]. The Xiaoerbulake Formation in the Tarim Basin has shown reserves of 75 billion m^3 of gas [16].

Recently, two key exploration wells in the Xinchang structural belt in the fourth member of the Leikoupo Formation in the Western Sichuan Basin of SW China (well Chuanke-1 and well Xinshen-1) produced a commercial gas flow at rates of 86.8×10^4 m^3/day and 68×10^4 m^3/day [35,36]. The well of the Pengzhou-1 in Jinma structural belt produced a commercial gas flow at a rate of 121.05×10^4 m^3/day. Soon after, the well of Yashen-1 and Yangshen-1 in the Yazihe-Shiyangchang structural belt produced a commercial gas flow at rates of 48.5×10^4 m^3/day and 60.32×10^4 m^3/day, respectively [34]. The success of the Xinchang and Pengzhou gas fields shows great reservoir conditions and an economic potential of microbial carbonates in the fourth member of the Leikoupo Formation in the Western Sichuan Basin of SW China.

Various studies have been conducted on sedimentary facies, sequence stratigraphy, reservoir characteristics, diagenesis, and the hydrocarbon accumulation model of the fourth member of the Leikoupo Formation in the Western Sichuan Basin [34,37–39]. Previous studies indicated that microbial carbonates, dominated by thrombolites and stromatolites, are mainly developed in tidal flat, and the distribution of them is controlled by a high-frequency sequence [40]. With respect to the mechanism of reservoir formation, Song [35] attributed it to karstification in the Indosinian Movement, while others emphasized the importance of early dolomitization and burial dissolution for reservoir formation [16,22,39]. However, the effects of syn-depositional dissolution on reservoir formation have been received less attention [41].

In this study, in order to clear out the formation mechanism of reservoirs in the Leikoupo Formation in Western Sichuan Basin of SW China, lithofacies, depositional environments, and diagenesis analyses were performed in samples collected from cores of 12 wells.

2. Geological Setting

The study area is located in the Northwestern Yangtze Block, adjacent to the Paleo-Tethys Ocean during the Anisian [42,43] (Figure 1a). Nowadays, the study area is located in the west of the Sichuan Basin (Figure 1b). The Anisian was a critical period for the transformation of the tectonic regime in the Sichuan Basin [42,44–46]. Before the Anisian, the western area of the Sichuan Basin was a passive continental margin [45], while at the end of the Middle Triassic, the Indosinian Movement led to the formation of the Luzhou paleo-uplift and Kaijiang paleo-uplift in the south and east of the Sichuan Basin [34,42]. After the Middle Triassic, the thrusting of the Longmen Mountain provided the Upper Triassic Xujiahe Formation with clastic rocks [42,47]. Due to the continuous thrust-orogeny, the present tectonic units of the Western Sichuan Basin are divided into 'two uplifts (Longmen Mountain and Xinchang), two slopes (Guanghan-Zhongjiang and Wenxing-Mianyang) and two depressions (Yuantong-Ande and Mianzhu)' [48] (Figure 1c).

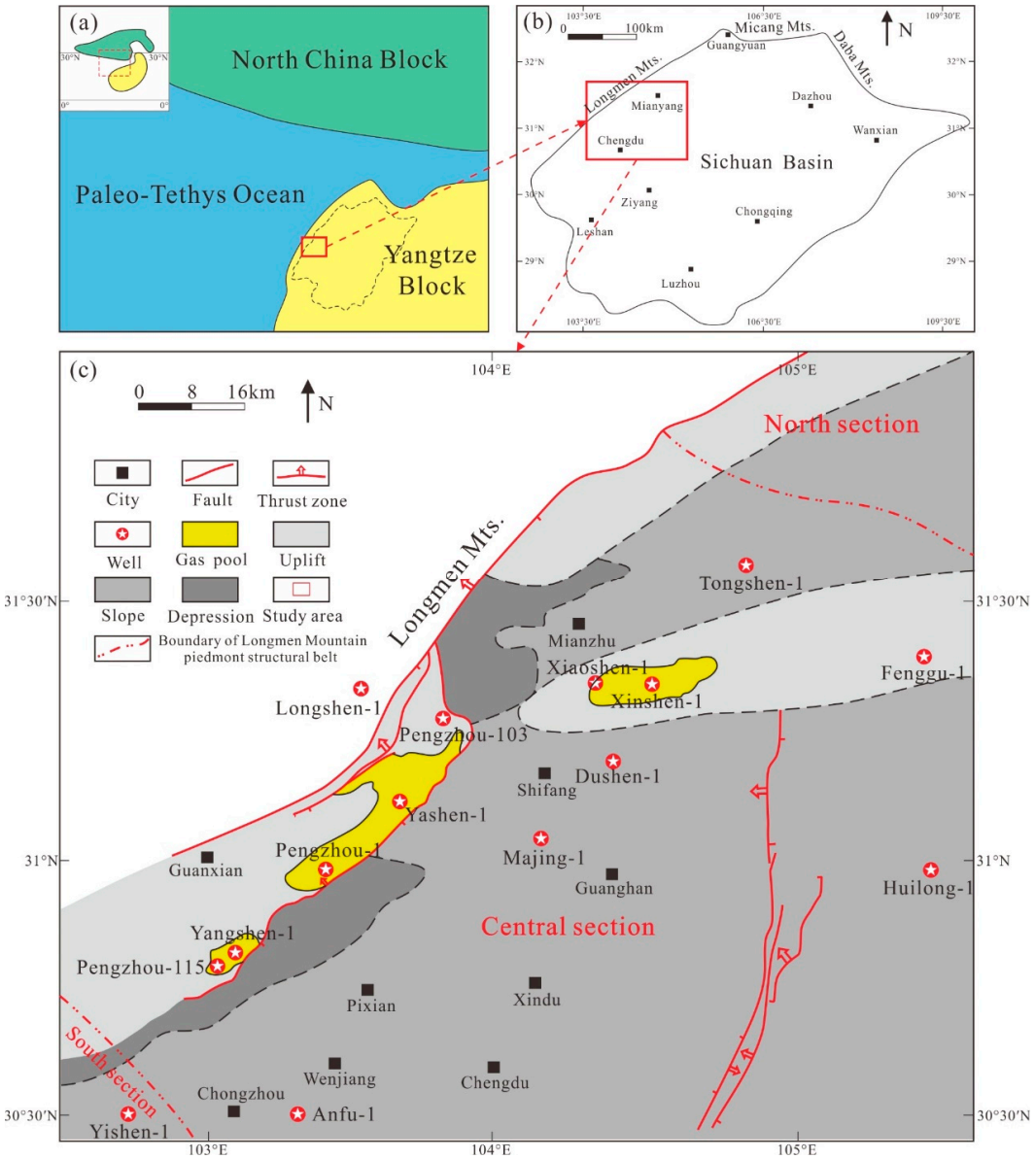

Figure 1. (**a**) The location of the study area in Middle Triassic. (**b**) The location of the study area in modern times. (**c**) The present tectonic units and representative wells of the study area (modified from [48]).

Under the control of the tectonic-sedimentary evolution, the Feixianguan Formation (the Lower Triassic), the Jianglingjiang Formation (the Lower Triaasic), the Leikoupo Formation (the Middle Triassic), the Ma'antang Formation (the Upper Triassic), and the Xujiahe Formation (the Upper Triassic) developed during the Triassic in the Western Sichuan Basin. The Leikoupo Formation was divided into four members, that is, from bottom to top, Lei-1 (T_2l_1), Lei-2 (T_2l_2), Lei-3 (T_2l_3), and Lei-4 (T_2l_4) [16,34,35] (Figure 2). Lei-4 was eroded to various degrees in the Western Sichuan Basin because of the Indosinian Movement, and the remaining thickness gradually decreased from west to east [49]. Lei-4 is mostly unconformably overlain by the Upper Triassic in the east and south of the Sichuan Basin, while in the west of the Sichuan Basin, especially in the Yazihe and Huanglianqiao areas, it is conformably overlain by the Tianjingshan Formation [34].

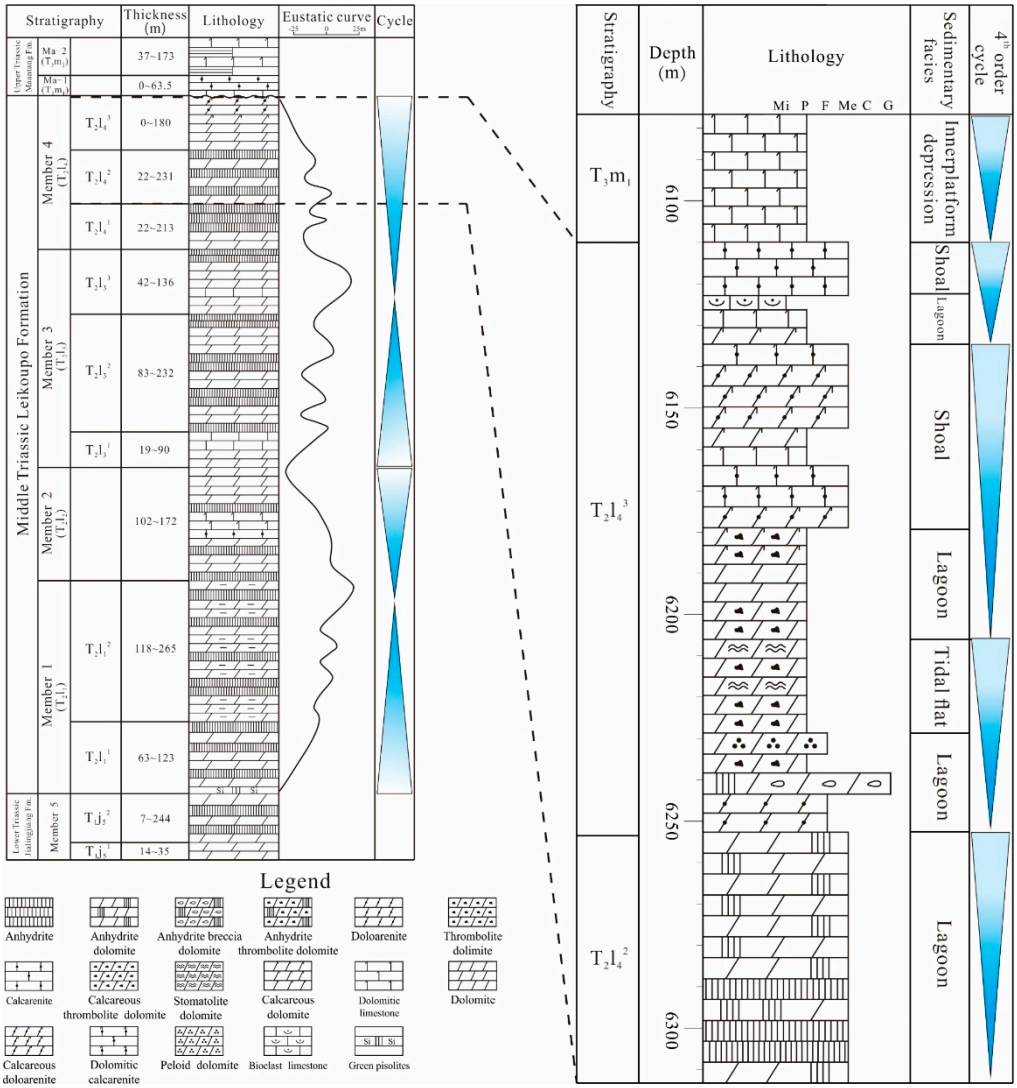

Figure 2. Sequence stratigraphy and lithology of the Leikoupo Formation in the Middle Triassic (modified from [34]), with an enlarged part showing the subdivision of the Member 4 of the Leikoupo Formation (Well Yangshen-1). $T_2l_1^1$ = lower sub-member of Lei-1; $T_2l_1^2$ = upper sub-member of Lei-1; T_2l_2 = Lei-2; $T_2l_3^1$ = lower sub-member of Lei-3; $T_2l_3^2$ = middle sub-member of Lei-3; $T_2l_3^3$ = upper sub-member of Lei-3; $T_2l_4^1$ = lower sub-member of Lei-4; $T_2l_4^2$ = middle sub-member of Lei-4; $T_2l_4^3$ = upper sub-member of Lei-4. 'Mi' = micrite; 'P' = powder; 'F' = fine; 'Me' = Medium; 'C' = coarse; 'G' = gravel.

The subduction of the Yangtze block caused the ancient Tethys Ocean to be gradually closed, and the seawater gradually withdrew from the Western Sichuan Basin in the NE–SW direction.

The climate was arid at this time. In such a climate, an evaporitic environment was developed, and the water body was restricted [50,51]. The total thickness of Lei-4 ranges from 144 to 2047 ft (44 to 624 m), and it can be divided into three sub-members, based on the different lithological associations (Figure 2). The lower Lei-4 ($T_2l_4^1$) has a thickness of 72–699 ft (22–213 m) and is dominated by thick anhydrite, anhydrite-dolomite, and dolomicrite, which are completely preserved in the Western Sichuan Basin. The middle Lei-4 ($T_2l_4^2$) is similar to the lower in terms of thickness (72–758 ft or 22–231 m). The lithology of the middle Lei-4 ($T_2l_4^2$) is composed of interbedded anhydrite and dolomicrite, and it is denuded in the east of the Well Huilong-1. The upper Lei-4 ($T_2l_4^3$) is 0–591 ft (0–180 m) in thickness and mainly consists of thrombolite, stromatolite, dolomitic limestone, calcarenite, and doloarenite, which tapers off toward the east.

3. Samples and Analytical Method

A total of 300 core samples were obtained from 12 wells in the study area (Figure 1). In one-third of the region, 300 thin sections were stained by Alizarin Red S to distinguish calcite and dolomite. Each thin section had a thickness of 0.03 mm and was impregnated with blue dye to reveal mega-pores.

Measurements on the microporosity were performed in 25 representative samples (the length, width, and height are all less than 3 mm) by a scanning electron microscope (FEI, USA), equipped with Energy Disperse Spectroscopy, (EDS) at the Key Laboratory of Orogenic Belts and Crustal Evolution, Peking University.

In order to quantificationally clarify the main pore type of the microbial reservoirs using the Image-J software, the percentage of each pore type area to the total pore area was counted through the following steps: (1) Representative images of thin casting sections with an area of 1.6×10^8 μm^2 (magnification of 50 times using a polarizing microscope) are taken; (2) the image analysis technology of Image-J is used to identify the pores and the total area of pores in the area, and the areal porosity is counted by $S_{pore}/S_{total} \times 100\%$; (3) different types of pores are artificially recognized, and the percentage of each pore type to the total pore area is counted by $S_{single\ pore}/S_{total\ pore} \times 100\%$.

For CL analysis, 40 selected samples were polished into thin Sections (0.06 mm thick) to identify the periods of cementation. Polarized light images were obtained using Leica DM2500P, and the CL images were acquired from CL8200 MK5 in a high vacuum field at the Petroleum Geology Research and Laboratory Center, Research Institute of Petroleum Exploration and Development, Petro China.

Powder samples of microbial carbonates were obtained for trace elements and rare earth elements (REE) at the Key Laboratory of Orogenic Belts and Crustal Evolution, Peking University. Of the powder samples, 250 mg were digested with 5 mL of HNO_3 for 1 h and then dried. Then, 10 mL of HNO_3 (1.42 g/mL) was added to the dried sample and heated at 130 °C for 2 h. Finally, an inductively coupled plasma-mass spectrometer (ICP-MS) was used to determine the contents of trace elements, including rare earth elements. ICP uses a high-frequency RF signal, applied to the inductor coil, to form a high-temperature plasma inside the coil. The high-temperature plasma ionizes all elements in the sample to form a monovalent positive ion and then transmits the monovalent positive ion to the mass spectrometer. The mass spectrometer can screen out ions with different ratios of mass to nuclear (m/z) and detect the intensity of each ion to analyze the intensity of each element. The values of rare earth elements are normalized to the Post-Archen Australian Shale (PAAS), published by Ali in 2012. The Eu and Ce anomaly values were calculated as follows: $\delta Eu = Eu^*/(0.5Sm^* + 0.5Gd^*)$, and $\delta Ce = Ce^*/(0.5La^* + 0.5Pr^*)$ [52].

Powder samples of microbial carbonates were selected for C and O isotopic measurements at the Key Laboratory of Orogenic Belts and Crustal Evolution, Peking University. The instrument was the IsoPrime 100 mass spectrometer, and the error of the results was within ±0.1‰. The test steps were as follows: (1) Every single sample is placed into a drying baker at 105 °C for 2 h to remove adsorbed water; (2) 20 mg of pure sample is weighed on the balance and put into the bottom of the reactor; (3) 4 mL anhydrous phosphoric acid is injected into the branch of the reactor, and the anhydrous phosphoric acid is heated at 60–70 °C for 2 h, until no more bubbles are produced; (4) the anhydrous

phosphoric acid and the sample reaction are made to release CO_2 at 25 °C for 36 h; (5) stable C and O isotopes are analyzed on an MAT 253 mass spectrometer; and (6) the C and O data are calibrated with the Vienna Peede Belemnite (VPDB) standard.

4. Results

4.1. Lithofacies Types

Based on the observation of the thin sections, sedimentary textures, sedimentary structures, and biotas association, ten lithofacies types were identified in Lei-4 of the Western Sichuan Basin (Table 1), including thrombolites (facies A), anhydritic thrombolites (facies B), stromatolites (facies C), bioclastic packstone (facies D), intraclast-dominated grainstone (facies E), microbial clot-dominated grainstone (facies F), peloid-dominated packstone to grainstone (facies G), anhydrite (facies H), dolomitic anhydrite (facies I), and crystalline carbonates (facies J).

4.1.1. Thrombolites

Thrombolites are comprehensive products of the capture from cyanobacteria or other archaea, self-calcification of microorganisms, precipitation of carbonates and diagenesis [53]. In this study, thrombolites (facies A) mainly developed in $T_2l_4^3$.

Core observations showed that the microbial adhesion structure (Figure 3a) developed in thrombolites, and a large number of pinholes and irregular dissolved pores, could be found (Figure 3b). Thin section observation under a microscope showed that two types of clots occurred in the thrombolites: an irregular-shaped clot, composed of uniform dolomicrite, without any obvious internal sedimentary structure; and an irregular-shaped clot bond of peloids (Figure 4a). Three types of benthic foraminifera were found in thrombolites: miliolinid foraminifera (Figure 4b), agglutinated textulariid foraminifera, with uniserially arranged chambers, and agglutinated textulariid foraminifera, with biserially arranged chambers. The typical Girvanella, a common cyanobacterium, could be found in the thrombolites (Figure 4c).

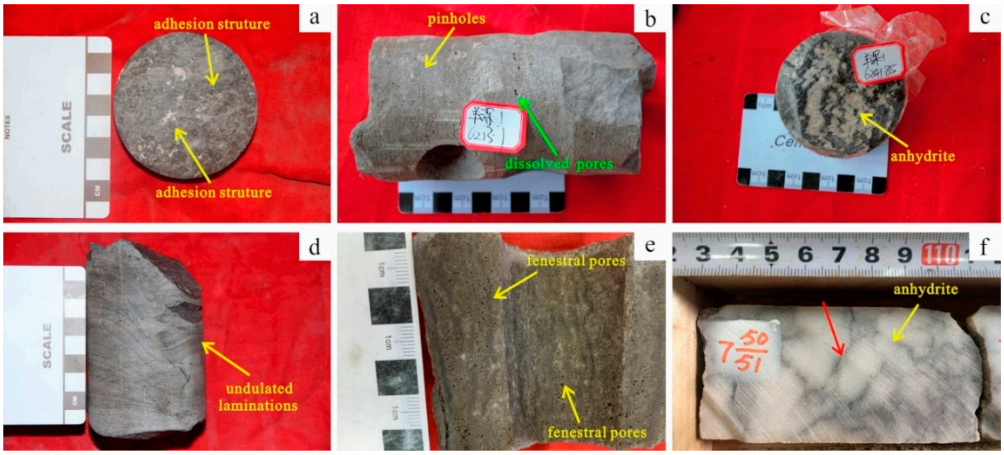

Figure 3. Macroscopic characteristics of the lithofacies types in the Leikoupo Formation. (**a**) Adhesion structure in thrombolites, $T_2l_4^3$, Pengzhou-103 well, 6045.20 m; (**b**) Pinholes (yellow arrow) and dissolved pores (green arrow) in thrombolites, $T_2l_4^3$, Yangshen-1 well, 6213.10 m; (**c**) Anhydrite filling in the original pores, $T_2l_4^2$, Yangshen-1 well, 6241.85 m; (**d**) Undulated laminations in stromatolites, $T_2l_4^3$, Longshen-1 well, 5990.26 m; (**e**) Fenestral pores in stromatolites, $T_2l_4^3$, Anfu-1 well, 5701.89 m; (**f**) Reticulated distribution of microbial dolomite in anhydrite (red arrow), $T_2l_4^2$, Anfu-1 well, 5716.71 m.

Table 1. Lithofacies types of the fourth member of the Leikoupo Formation in the Western Sichuan Basin.

	Lithofacies	Sedimentary Texture	Types of Grains	Size of Grains/Crystal	Palaeontologic Association	Description	Water Energy	Depositional Environment
A	Thrombolites	Microbial clotted fabric	Few peloids	Micrite (clot) Silt (peloid)	Miliolinid foraminifera Textulariid foraminifera (single chamber and biserial chamber)	Moderate dolomitization, micrite to silt crystal, irregular shaped clots and spheriform peloid	Low to medium	Shallow subtidal, intertidal
B	Anhydritic thrombolites	Microbial clotted fabric	Few peloids	Micrite (clot) Silt (peloid)	A few miliolinid foraminifera	Strong dolomitization, micrite to silt crystal, fully cemented by anhydrite	Low	Lagoon
C	Stromatolites	Microbial laminated structure	Few peloids	Micrite (lamination) Silt (peloid)	A few miliolinid foraminifera	Strong dolomitization, micrite to silt crystal, slightly undulated laminations	Medium to high	Microbial mounds
D	Bioclastic packstone	Grain-supported	Bioclasts	Silt (bioclasts)	Mainly miliolinid foraminifera and few shells	Weak dolomitization, micrite crystal	Low	Lagoon
E	Intraclast-dominated grainstone	Grain-supported	Intraclasts (primary) Isolated microbial clots Peloids	Silt-fine (intraclasts) Fine-coarse (microbial clots) Fine (peloids)	Few miliolinid foraminifera	Moderate dolomitization, silt to fine, fully cemented by calcite or dolomite	High	Shoal (intertidal)
F	Microbial clot-dominated grainstone	Grain-supported	Isolated microbial clots (primary) Intraclasts Peloids	Fine-coarse (microbial clots) Silt-fine (intraclasts) Silt (peloids)	Few miliolinid foraminifera	Moderate dolomitization, silt to coarse, fully cemented by calcite or dolomite	High	Shoal (intertidal)
G	Peloid-dominated packstone to grainstone	Grain-supported	Peloids (primary) Intraclasts	Silt (peloids) Silt-fine (intraclasts)	Few miliolinid foraminifera	Moderate dolomitization, silt to fine, fully cemented by calcite or dolomite	Medium	Lagoon, intertidal

Table 1. *Cont.*

	Lithofacies	Sedimentary Texture	Types of Grains	Size of Grains/Crystal	Palaeontologic Association	Description	Water Energy	Depositional Environment
H	Anhydrite	Crystalline texture	None	Medium-fine (anhydrite)	None	Medium to fine crystal, dense cementation	Low	Lagoon
I	Dolomitic anhydrite	Crystalline texture	None	Medium-fine (anhydrite) Micrite (microbial filaments)	None	Medium to fine crystal, dense cementation, filamentous microbial structure	Low	Lagoon
J	Crystalline carbonates	Crystalline texture	None	Micrite-fine (dolomite) Micrite (calcite)	None	Moderate dolomitization, micrite to silt, residual microbial texture	Low to medium	Lagoon, intertidal

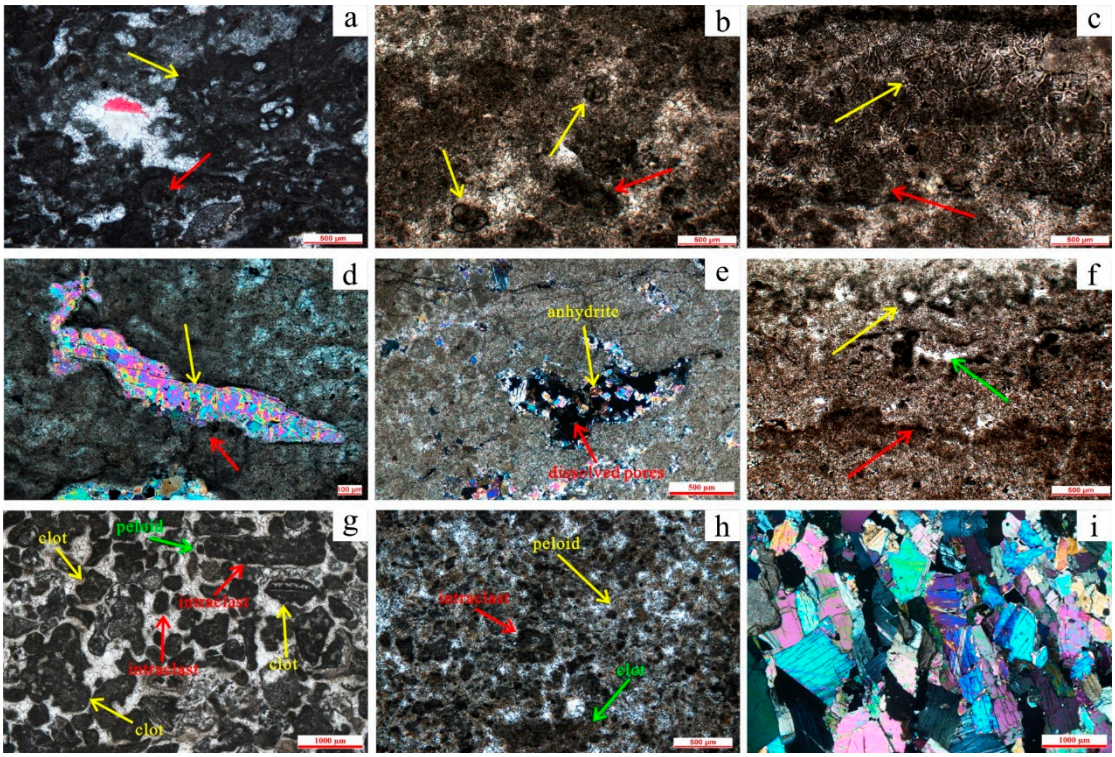

Figure 4. Microscopic characteristics of lithofacies types in the Leikoupo Formation. (**a**) Two kinds of clots in thrombolites: The clot composed of uniform dolomicrite (yellow arrow), and the clot bond of peloids (red arrow), $T_2l_4^3$, Yangshen-1 well, 6199.50 m; (**b**) Miliolinid foraminifera (yellow arrow) and microbial clots (red arrow), $T_2l_4^3$, Pengzhou-103 well, 6022.14 m; (**c**) Girvanella (yellow arrow) of cyanobacterium and microbial clots (red arrow), $T_2l_4^3$, Pengzhou-115 well, 6316.00 m; (**d**) Anhydrite fully filling in the original pores (yellow arrow) and microbial clots (red yellow), $T_2l_4^3$, Xinshen-1 well, 5628.80 m; (**e**) Residual anhydrite with irregular edge in dissolved pores, $T_2l_4^3$, Tongshen-1 well, 5850.22 m; (**f**) Two kinds of laminations in stromatolites: The lamination made up of dolomicrite (red arrow), and the lamination composed of peloids and clots (yellow arrow), and the fenestral pores can also be found (green arrow), $T_2l_4^3$, Yishen-1 well, 5891.28 m; (**g**) Three types of grains in in facies F, intraclast (red arrow), clot (yellow arrow) and peloid (green arrow), $T_2l_4^3$, Yangshen-1 well, 6119.98 m; (**h**) Three types of grains in facies G, intraclast (red arrow), peloid (yellow arrow) and clot (green arrow), $T_2l_4^3$, Yangshen-1 well, 6235.90 m; (**i**) Anhydrite in facies H, medium to fine crystal, $T_2l_4^2$, Longshen-1 well, 6720.10 m.

Another type of thrombolite is anhydritic thrombolites (facies B), which was developed mainly in $T_2l_4^1$ and $T_2l_4^2$. The characteristics of the clots in the anhydritic thrombolites were similar to these in the former types of thrombolites, while in the inter-particle pore space, they were mostly full of anhydrite (Figures 3c and 4d). In the Tongshen-1 well, the anhydrite in the pores was partially dissolved, and residual anhydrite with an irregular edge could be found in the pores (Figure 4e).

4.1.2. Stromatolites

Stromatolites were mainly developed in $T_2l_4^3$ and were easy to recognize from the cores because of their slightly undulated laminations (Figure 3d). A large number of fenestral pores could be found in the core (Figure 3e). The alternation of dark and light dolomite (millimeters in thickness for a single lamination) showed that the stromatolites often developed in an environment where water energy changes frequently. There are two types of undulate laminations in stromatolites. One is made up of dolomicrite, and the other is composed of peloids and clots, while both can be found in one single lamination occasionally (Figure 4f).

4.1.3. Bioclastic Packstone

A large number of benthic foraminifera (dominated by miliolinid foraminifera) and a few fragments of shells could be found in bioclastic packstone. Besides, it contained a small number of peloids. The matrix was primarily dolomicrite, and little pore space occurred in bioclastic packstone.

4.1.4. Grainstone

Three types of grainstone were found in $T_2l_4^3$: intraclast-dominated grainstone (facies E), microbial clot-dominated grainstone (facies F) (Figure 4g) and peloid-dominated packstone to grainstone (facies G) (Figure 4h). However, in general, these three kinds of grainstones coexist in a sample. The intraclasts were composed of uniform dolomicrite and subrounded in sizes of 100 to 300 μm. The microbial clots were isolated and differed from the intraclasts by their irregular shape and internal agglutinated structure of microorganisms, and they were generally larger than intraclasts and peloids, with sizes ranging mainly between 200 to 1500 μm. The peloids were subrounded or rounded, had a good sorting, were composed of uniform dolomicrite, and commonly exhibited a diameter from 30 to 80 μm. Some inter-particle pores were found in grainstones. The pore sizes of intraclast-dominated grainstone and microbial clot-dominated grainstone were mainly tens of microns, while the pores in peloid-dominated grainstone had a size of hundreds of nanometers to several microns.

4.1.5. Anhydrite and Dolomitic Anhydrite

Anhydrite (facies H) and dolomitic anhydrite (facies I) developed mainly in $T_2l_4^1$ and $T_2l_4^2$. The anhydrite shows milky white in the cores, while dolomite shows dark grey and had a reticulated distribution in anhydrite (Figure 3f). Observation under a microscope suggested that the anhydrite crystals were platy or had an irregular shape, and the reticulated dolomite turned out to be formed by microorganism activities (Figure 4i). Little pore space could be found in anhydrite and dolomitic anhydrite.

4.1.6. Crystalline Carbonates

Crystalline carbonates (facies J) developed mainly in the upper sub-member of Lei-4. The calcite was mainly less than 1 μm, and the dolomite displayed a wide range of crystal sizes, from 1 μm to 250 μm. The residual microbial texture could be found in silt crystal dolomite.

4.2. Characteristics of Microbial Carbonate Reservoirs

4.2.1. Pore Types

Six types of pores were identified in $T_2l_4^3$: inter-clot pores, fenestral pores, intra-clot pores, inter-crystal pores, micropores, and fractures. The terminology of pore types refers to the pore classification scheme of carbonates proposed by Moore [54].

The inter-clot pores in $T_2l_4^3$ were well developed in facies A and facies B, in which the particles were mainly interconnected microbial clots, and the pores had irregular shapes, with sizes ranging from tens to hundreds of microns (Figure 5a,e). Dolomite cements grew close to the clots and occupied part of pore space. The rest of the pore space was either filled with calcite cements or preserved without any fillings.

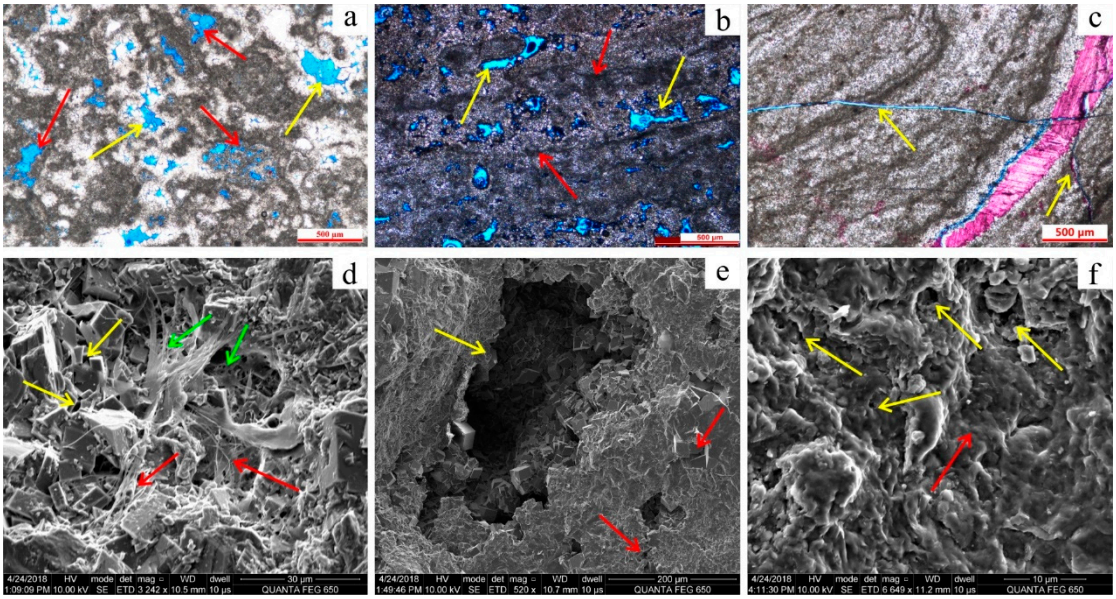

Figure 5. Microscopic characteristics of the pore types in the Leikoupo Formation. (**a**) Inter-clot pores (yellow arrow) and intra-clot pores (red arrow) in thrombolites, $T_2l_4^3$, Yangshen-1 well, 6228.60 m; (**b**) Fenestral pores (yellow arrow) directionally along the laminations (red arrow) in stromatolites, $T_2l_4^3$, Yishen-1 well, 5886.80 m; (**c**) Fractures (yellow arrow) in stromatolites, $T_2l_4^3$, Yashen-1 well, 5788.78 m; (**d**) Inter-crystal micropores (yellow arrow), filiform microbes (red arrow) and micropores in filiform microbes (green arrow) in stromatolites, $T_2l_4^3$, Yangshen-1 well, 6207.10 m; (**e**) Inter-clot pores (yellow arrow) and inter-crystal pores (red arrow) in thrombolites, $T_2l_4^3$, Yangshen-1 well, 6228.60 m; (**f**) Inter-particle pores (micropores, yellow) and peloids (red arrow), $T_2l_4^3$, Longshen-1 well, 5971.46 m.

Fenestral pores were mainly developed in facies C. The pores were developed directionally along the laminations, with a size of 50 to 1500 μm (Figure 5b). The shape of the fenestral pores was irregular and narrow. Abundant pore space was preserved, although few dolomite and quartz cements filled in the pore space.

Intra-clot pores were observed in facies A and facies B, which were formed in microbial clots, with sizes ranging from 2 to 15 μm (Figure 5a).

Both structural fractures and dissolution fractures were generally developed in facies A and facies F. The aperture of the structural fractures was mainly from 0.01 to 0.2 mm (Figure 5c). Dissolution fractures were mainly 0.1~0.3 mm in aperture and were enlarged by the dissolution in a partial position of the fractures.

Inter-crystal pores were mainly developed in facies A and facies C (Figure 5d). While inter-crystal pores represented a smaller proportion of the total porosity than inter-particle pores (between interconnected microbial clots), this type of pore was widely developed in microbial carbonate rocks. Inter-crystal pores were 5 to 15 μm in size, and little cement was formed in the pore space.

Micropores were observed in facies A, facies C, and facies G, and they were clearly recognized under SEM observation. The types of micropores were mainly inter-crystal pores, inter-particle pores, and microbial pores which developed between filaments of microbes, with a size of 200 nm to 1 μm (Figure 5d,f).

4.2.2. Physical Properties

The petrophysical data, including porosity and permeability, were obtained from 12 wells. On the whole, the microbial reservoirs of Lei-4 had the characteristics of a medium-low porosity and low permeability, based on statistics from 347 samples (Figure 6). The physical properties varied with lithofacies. The microbial carbonates had a better reservoir quality than grainstone, bioclastic packstone, and anhydrite. In the microbial carbonates, the porosity of thrombolites ranged from 0.26 to 23.7%,

with an average of 3.77%. The average porosity of limestone was 0.76%, while average porosity of dolomite was 4.8%. This shows that dolomite had a better reserve capacity than limestone in Lei-4. While the stromatolites had a high porosity of 7.02%.

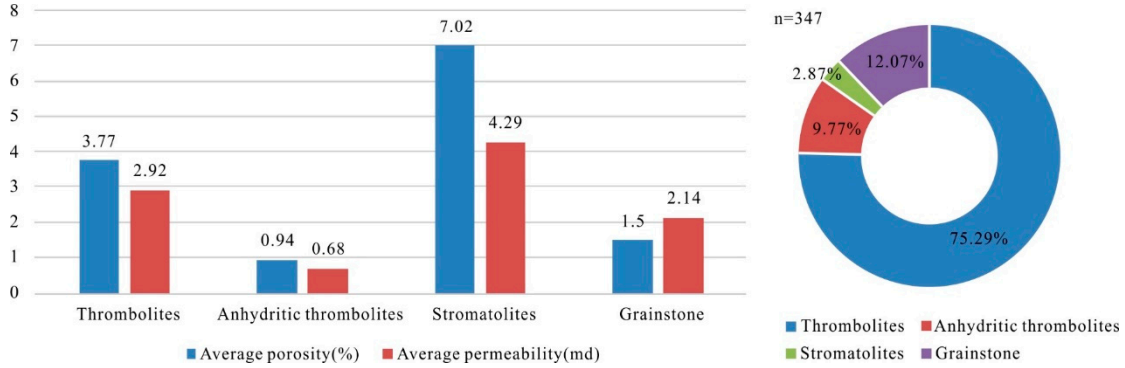

Figure 6. Average porosity, average permeability and frequency of different lithofacies in the Leikoupo Formation. The number of samples is 347.

The analysis of main pore types in thrombolites was carried out using the software, Image-J (Figure 7). The main pore types of thrombolites were inter- clot pores, intra-clot pores and inter-crystal pores. According to the statistics results (Table 2), the inter-crystal pores had an average area of 0.12×10^6 μm^2, accounting for 8.71% of the total pores. The average area of the intra-clot pores was 0.07×10^6 μm^2, accounting for 6.40% of the total pores, while the average area of the inter-clot pores was 1.23×10^6 μm^2, accounting for 84.89% of the total pores, which indicates that inter-clot pores were the dominant pore type of the microbial reservoir.

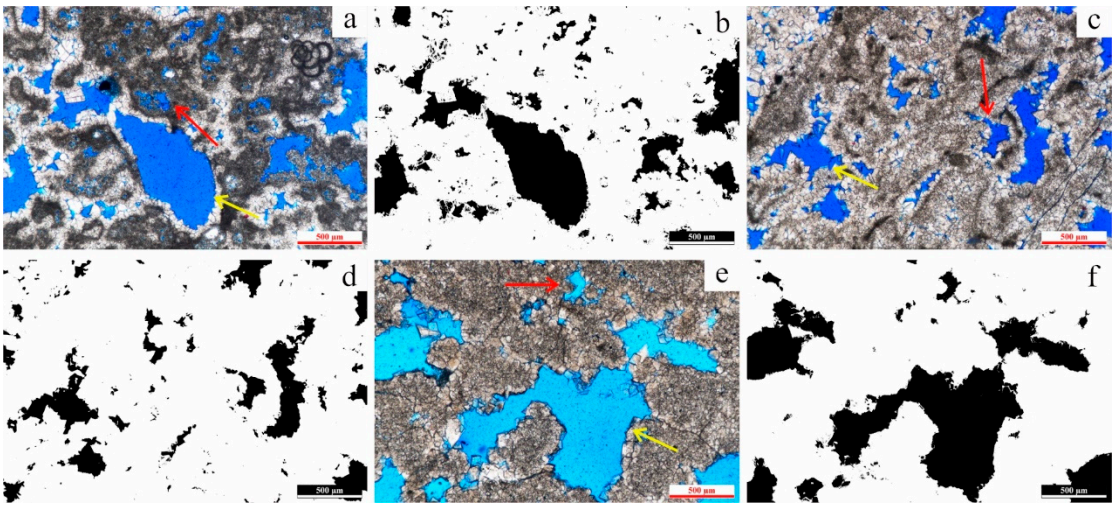

Figure 7. Comparison of the original image of thin sections generated by the Image-J software. (**a**) Inter-clot pores (yellow arrow) and intra-clot pores (red arrow) in thrombolites, $T_2l_4^3$, Yangshen-1 well, 6228.60 m; (**b**) Comparison image with a: The black area represents the pores, and the white area stands for the matrix; (**c**) Inter-clot pores (yellow arrow) and intra-clot pores (red arrow) in thrombolites, $T_2l_4^3$, Yangshen-1 well, 6222.30 m; (**d**) Comparison image with c: The black area represents the pores, and the white area stands for the matrix; (**e**) Inter-clot pores (yellow arrow) and intra-clot pores (red arrow) in thrombolites, $T_2l_4^3$, Yangshen-1 well, 6219.50 m; (**f**) Comparison image with (**e**): The black area represents the pores, and the white area stands for the matrix.

4.3. Geochemical Characteristics

4.3.1. Redox-Sensitive Trace Elements

The values of Th, U, V, Ni, Mn, Sr, and Co of the microbial carbonates (thrombolites and stromatolites) and grainstone are shown in Table 3. The Mn/Sr ratio of all the samples varied from 0.00 to 0.81 (average: 0.114). The Th/U and V/(V + Ni) ratios of thrombolites varied from 0.00 to 0.17 (average: 0.03) and from 0.20 to 0.93 (average: 0.73), respectively. The Th/U and V/(V+Ni) ratios of stromatolites varied from 0.01 to 0.10 (average: 0.02) and from 0.52 to 0.88 (average: 0.76), respectively. The Th/U and V/(V + Ni) ratios of grainstone varied from 0.00 to 0.01 (average: 0.01) and from 0.72 to 0.88 (average: 0.78), respectively. As for the Ni/Co ratios, the thrombolites varied from 8.02 to 20.18 (average: 12.31), the stromatolites varied from 9.81 to 14.60 (average 11.94), and the grainstone varied from 10.93 to 13.38 (average: 12.06).

The diagenetic alteration may have affected the representativeness of the carbonate samples of seawater, and the diagenetic alteration process of marine carbonate was a process of manganese acquisition and strontium loss [55–57]. Therefore, the concentrations of Mn and Sr and the ratio of Mn/Sr were used to determine the degree of diagenetic alteration. In general, carbonates with Mn/Sr < 10 retained their original seawater geochemical conditions, especially for Mn/Sr < 2–3 [58,59]. In this study, the average Mn/Sr ratio of all the samples was 0.114 (far less than 2), which indicated that their geochemical data could represent the original redox conditions of depositional environments.

Th/U, V/V+Ni, and Ni/Co were used to determine palaeo-redox conditions [59–62]. Concretely speaking, Th/U ratios < 1.5 imply anoxic conditions, Th/U ratios ranging from 1.5 to 3 manifest dysoxic conditions, and Th/U ratios > 3 suggested oxic conditions [59–61]. Hatch and Leventhal [60] suggested V/(V + Ni) ratios > 0.84 for euxinic conditions, 0.54–0.82 for anoxic waters, and 0.46–0.60 for dysoxic conditions. As for Ni/Co ratios, Jones and Manning [61] suggested that Ni/Co ratios < 5 imply oxic conditions, ratios ranging from 5 to 7 indicate dysoxic conditions, and ratios > 7 manifest anoxic conditions. The average Th/U ratios of all the samples in Lei-4 was 0.023 (far less than 1.5), the average V/(V + Ni) ratios of thrombolites, stromatolites, and grainstone were 0.73, 0.76 and 0.78 (between 0.54 and 0.82), respectively, and the average Ni/Co ratios of all the samples was 12.18 (more than 7) (Table 3), all of which indicated anoxic conditions.

4.3.2. Rare Earth Elements

The values of rare earth elements (REE) are presented in Table 4 and Figure 8. The ∑REE of microbial carbonates (thrombolites and stromatolites) and grainstone varied from 0.50 to 3.32 (average: 1.20), which is two magnitudes lower than the average ∑REE of PAAS (184.77 μg/g). This indicates that the sediments in T_2l_4 were weakly affected by terrigenous clasts during the sedimentary process or diagenesis [52]. The ∑LREE (light rare earth elements)/∑HREE (heavy rare earth elements) varied from 0.70 to 8.07 (average: 1.87), which indicated that the LREE were lightly enriched, and HREE were lightly depleted. Almost all samples of the Leikoupo Formation displayed a positive Eu anomaly. The samples of lithofacies G and J displayed a slightly positive Ce anomaly, while the microbialites samples displayed a slightly negative Ce anomaly.

4.3.3. Stable Carbon and Oxygen Isotopes

The results of stable C and O isotopes are presented in Table 5 and Figure 9. The $\delta^{18}O_{VPDB}$ value of limestone was between −8.43‰ and −7.02‰, the $\delta^{13}C_{VPDB}$ values were between 1.09‰ and 2.25‰, and the $\delta^{18}O_{VPDB}$ value of dolomite ranged from −9.97‰ to −3.50‰ and from 2.16‰ to 3.75‰ for the $\delta^{13}C_{VPDB}$ values. The $\delta^{18}O_{VPDB}$ value of thrombolites was between −9.55‰ and −3.50‰ and between 1.89‰ and 3.75‰ for the $\delta^{13}C_{VPDB}$ values. The $\delta^{18}O_{VPDB}$ value of stromatolites ranged from −9.97‰ to −6.02‰ and from 2.32‰ to 2.69‰ for the $\delta^{13}C_{VPDB}$ values. The $\delta^{18}O_{VPDB}$ value of grainstone was between −7.95‰ and −5.77‰, and the $\delta^{13}C_{VPDB}$ values were between 1.09‰ and 2.77‰. In general, thrombolites displayed the highest isotopic range for both the $\delta^{18}O_{VPDB}$ and

$\delta^{13}C_{VPDB}$ values, grainstone displayed the lowest range for the $\delta^{18}O_{VPDB}$ values, and stromatolites displayed the lowest range for the $\delta^{13}C_{VPDB}$ values.

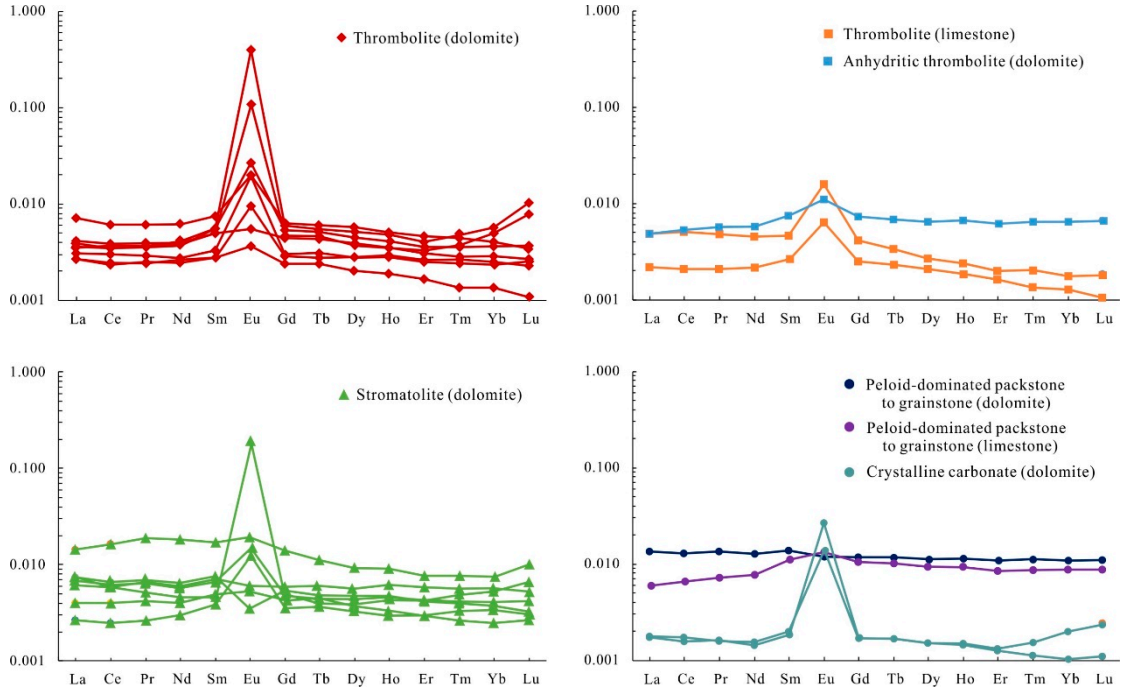

Figure 8. Rare earth elements (REE) pattern of different lithofacies in the Leikoupo Formation. The values of rare earth elements are normalized to the Post-Archen Australian Shale (PAAS).

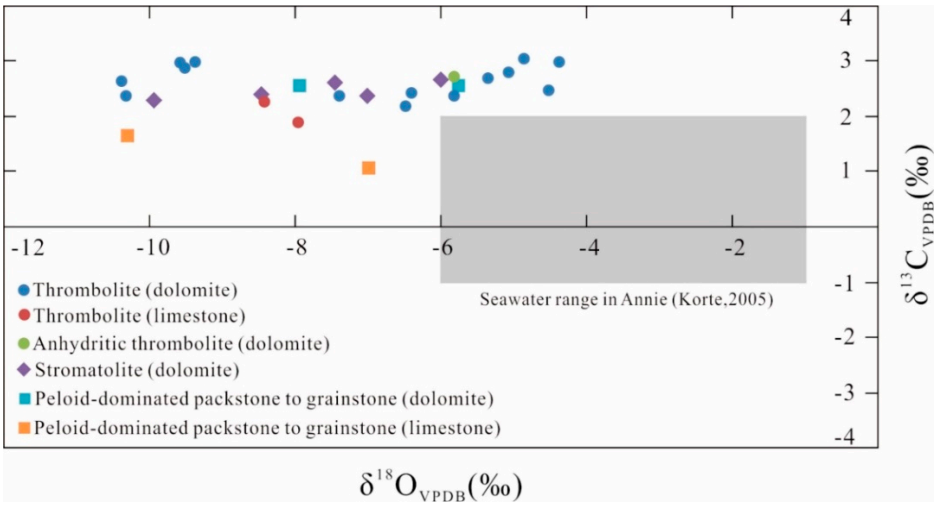

Figure 9. Carbon and oxygen isotopic compositions of different lithofacies in the Leikoupo Formation. VPDB = Vienna Peedee Belemnite.

Table 2. Statistics of the area percentage of different types of pores in the fourth member of the Leikoupo Formation.

Well	Depth(m)	Areal Porosity (%)	Total Area of Pores ($\times 10^6$ μm^2)	Area of Inter-Clot Pores ($\times 10^6$ μm^2)	Area Percentage of Inter-Clot Pores (%)	Area of Intra-Clot Pores ($\times 10^6$ μm^2)	Area Percentage of Intra-Clot Pores (%)	Area of Inter-Crystal Pores ($\times 10^6$ μm^2)	Area Percentage of Inter-Crystal Pores (%)
XS-1	5549.2	9.52	1.52	1.24	81.87	0.15	9.61	0.13	8.52
XS-1	5551.2	7.75	1.24	1.08	86.91	0.00	0.00	0.16	13.09
YaS-1	5781.7	3.84	0.49	0.43	89.08	0.00	0.00	0.05	10.93
YaS-1	5782.6	9.73	1.56	1.46	93.75	0.00	0.00	0.10	6.25
YaS-1	5782.9	7.22	1.16	1.03	88.78	0.03	2.45	0.10	8.77
YS-1	6219.5	17.31	2.77	2.62	94.57	0.04	1.47	0.11	3.96
YS-1	6222.3	13.26	2.15	1.80	83.97	0.20	9.32	0.14	6.71
YS-1	6228.6	13.78	0.73	0.42	57.16	0.29	39.24	0.03	3.60
YS-1	6191.4	10.33	1.65	1.47	88.83	0.00	0.00	0.18	11.17
YS-1	6191.9	5.80	0.93	0.78	83.96	0.02	1.95	0.13	14.09
Average		9.85	1.42	1.23	84.89	0.07	6.40	0.11	8.71

Table 3. Values of the redox-sensitive trace elements in the fourth member of the Leikoupo Formation.

Depth (m).	Well	Lithofacies	Th (ppm)	U (ppm)	V (ppm)	Ni (ppm)	Mn (ppm)	Sr (ppm)	Co (ppm)	Mn/Sr	Th/U	V/V + Ni	Ni/Co
6228.60	YS1	Facies A	0.02	4.69	9.09	1.49	19.88	134.79	0.14	0.15	0.01	0.86	10.39
6222.30	YS1	Facies A	0.01	4.56	18.66	1.42	15.52	117.78	0.15	0.13	0.00	0.93	9.51
5779.00	YaS1	Facies A	0.02	6.60	15.98	3.98	13.24	65.32	0.29	0.20	0.00	0.80	13.66
5782.90	YaS1	Facies A	0.07	7.80	54.40	3.82	15.22	65.84	0.34	0.23	0.01	0.93	11.40
5551.20	XS1	Facies A	0.05	3.76	12.42	4.08	9.43	98.65	0.32	0.10	0.01	0.75	12.75
5982.38	LS1	Facies A	0.13	3.30	10.44	4.63	6.03	141.63	0.38	0.04	0.04	0.69	12.20
5785.90	YaS1	Facies A	0.12	3.86	13.80	4.25	13.87	94.50	0.37	0.15	0.03	0.77	11.47
6045.57	PZ103	Facies A	0.03	4.79	20.94	9.89	12.16	135.53	0.49	0.09	0.01	0.68	20.18
5976.53	LS1	Facies A	0.11	5.87	11.96	5.31	5.16	95.97	0.44	0.05	0.02	0.69	12.14
5729.30	YaS1	Facies A	0.15	2.91	22.32	4.68	2.95	64.19	0.58	0.05	0.05	0.83	8.02
5730.20	YaS1	Facies A	0.01	2.36	14.30	8.16	2.12	260.60	0.63	0.01	0.01	0.64	12.95
5628.80	XS1	Facies B	0.03	0.14	1.58	6.32	0.00	3220.69	0.45	0.00	0.17	0.20	14.05
5987.48	LS1	Facies A	0.21	5.45	9.75	5.91	2.77	104.94	0.72	0.03	0.04	0.62	8.16
5970.82	LS1	Facies A	0.01	11.10	21.47	5.64	5.06	99.14	0.42	0.05	0.00	0.79	13.48
5978.86	LS1	Facies A	0.04	5.44	17.10	5.49	3.45	65.04	0.38	0.05	0.01	0.76	14.30
6207.10	YS1	Facies C	0.07	7.19	41.11	5.53	16.10	114.79	0.55	0.14	0.01	0.88	10.10
5826.50	PZ1	Facies C	0.39	3.93	20.21	4.63	11.87	94.59	0.47	0.13	0.10	0.81	9.81
6219.50	YS1	Facies C	0.02	1.95	8.00	3.99	13.53	107.45	0.32	0.13	0.01	0.67	12.35
5986.08	LS1	Facies C	0.06	5.85	12.02	5.49	4.95	94.01	0.45	0.05	0.01	0.69	12.09

Table 3. *Cont.*

Depth (m).	Well	Lithofacies	Th (ppm)	U (ppm)	V (ppm)	Ni (ppm)	Mn (ppm)	Sr (ppm)	Co (ppm)	Mn/Sr	Th/U	V/V + Ni	Ni/Co
5717.60	XaS1	Facies C	0.03	3.90	33.85	5.14	14.87	189.17	0.46	0.080	0.01	0.87	11.30
5990.46	LS1	Facies C	0.02	3.55	6.17	5.77	3.11	99.77	0.43	0.03	0.01	0.52	13.31
5979.54	LS1	Facies C	0.08	8.55	48.15	8.45	4.594	107.51	0.58	0.04	0.01	0.85	14.60
6185.60	YS1	Facies G	0.04	3.81	15.28	5.24	10.36	164.57	0.44	0.06	0.01	0.75	11.87
6234.90	YS1	Facies G	0.00	2.68	10.13	4.03	7.88	127.69	0.30	0.06	0.00	0.72	13.38
5711.10	XaS1	Facies G	0.09	6.86	40.76	5.35	100.93	124.56	0.49	0.81	0.01	0.88	10.93

Table 4. Values of rare earth elements of different lithofacies in the fourth member of the Leikoupo Formation.

Sample	Well	Depth (m)	Lithofacies	Elemental Mass Fraction ($\times 10^{-3}$ μg·g^{-1}, PAAS)														∑REE (μg·g^{-1}, PAAS)	∑LREE/∑HREE (PAAS)	δCe	δEu
				La	Ce	Pr	Nd	Sm	Eu	Gd	Tb	Dy	Ho	Er	Tm	Yb	Lu				
6228.6	YS1	6228.60	Facies A	7	6	6	6	7	19	6	6	6	5	5	4	4	3	0.091	1.298	0.943	2.851
6222.3	YS1	6222.30	Facies A	4	4	4	4	5	27	5	5	5	4	4	4	4	4	0.081	1.403	0.932	5.091
5779	Ya1	5779.00	Facies A	3	2	2	3	3	10	3	3	3	3	3	3	2	2	0.044	1.055	0.942	3.430
5782.9	Ya1	5782.90	Facies A	4	4	4	4	5	101	5	5	4	4	3	4	5	8	0.158	3.317	0.931	21.093
5551.2	XS1	5551.20	Facies A	4	3	4	4	5	352	6	6	5	5	4	5	6	10	0.418	8.074	0.914	63.876
LS1-38	LS1	5982.38	Facies A	3	2	2	2	3	4	2	2	2	2	2	1	1	1	0.031	1.165	0.920	1.428
PZ103-2	PZ103	6045.57	Facies A	3	3	3	3	3	19	3	3	3	3	3	2	2	3	0.056	1.595	1.030	6.168
LS1-46	LS1	5976.53	Facies A	4	4	4	4	5	6	4	4	4	4	3	3	3	3	0.054	0.959	0.936	1.217
LS1-53	LS1	5970.82	Facies A	5	5	5	5	5	16	4	3	3	2	2	2	2	2	0.059	1.954	1.084	3.909
LS1-43	LS1	5978.86	Facies A	2	2	2	2	3	6	2	2	2	2	2	1	1	1	0.031	1.244	0.938	2.508
6224.21	YS1	6224.21	Facies B	5	5	6	6	8	11	7	7	7	7	6	7	6	7	0.093	0.759	0.981	1.495
6207.1	YS1	6207.10	Facies C	6	6	7	6	7	6	6	6	6	6	6	6	6	5	0.084	0.838	0.932	0.895
5826.5	PZ1	5826.50	Facies C	14	16	19	19	17	19	14	11	9	9	8	8	8	10	0.181	1.361	0.995	1.335
6219.5	YS1	6219.50	Facies C	7	6	5	5	5	179	4	4	4	4	4	5	5	7	0.244	5.494	0.998	41.305
LS1-31	LS1	5986.08	Facies C	4	4	4	4	5	5	4	4	4	3	3	3	2	3	0.053	0.986	1.010	1.144
5717.6	XaS1	5717.60	Facies C	3	2	3	3	4	13	4	4	3	3	3	3	3	3	0.054	1.039	0.877	3.347
LS1-24	LS1	5990.46	Facies C	7	6	7	6	7	3	5	5	5	5	4	4	4	3	0.072	1.092	0.961	0.559
LS1-48	LS1	5979.54	Facies C	7	6	7	6	7	15	5	4	4	5	4	4	4	4	0.082	1.351	0.986	2.740
6185.6	YS1	6185.60	Facies G	13	13	13	13	14	12	12	12	11	12	11	11	11	11	0.168	0.866	0.971	0.952
5711.1	XaS1	5711.10	Facies G	6	7	7	8	11	13	10	10	9	9	9	9	9	9	0.126	0.698	0.971	1.175
5725.2	YaS1	5725.20	Facies J	2	2	2	1	2	26	2	2	2	1	1	2	2	2	0.048	2.559	1.010	14.666
5767.8	YaS1	5767.80	Facies J	2	2	2	2	2	14	2	2	2	1	1	1	1	1	0.033	2.053	1.052	7.495

Table 5. Values of stable carbon and oxygen isotopes of different lithofacies in the fourth member of the Leikoupo Formation.

Sample	Well	Depth(m)	Lithofacies	$\delta^{18}O_{(VPDB)}$ (‰)	$\delta^{13}C_{(VPDB)}$ (‰)	Porosity (%)
6228.6	YS1	6228.60	Facies A (Dolomite)	−6.41	2.43	7.16
6222.3	YS1	6222.30	Facies A (Dolomite)	−5.36	2.68	5.19
5779	YaS1	5779.00	Facies A (Dolomite)	−9.55	2.93	2.1
5782.9	YaS1	5782.90	Facies A (Dolomite)	−9.38	2.99	5.7
5551.2	XS1	5551.20	Facies A (Dolomite)	−4.88	3.04	6.3
LS1-38	LS1	5982.38	Facies A (Dolomite)	−4.52	2.48	1.28
5782.6	YaS1	5782.60	Facies A (Dolomite)	−10.39	2.65	5.7
5820.6	PZ1	5820.60	Facies A (Dolomite)	−10.31	2.38	14.2
5785.9	YaS1	5785.90	Facies A (Dolomite)	−9.52	2.88	8.1
PZ103-2	PZ103	6045.57	Facies A (Dolomite)	−4.38	2.99	4.7
LS1-46	LS1	5976.53	Facies A (Dolomite)	−5.83	2.36	1.42
5729.3	YaS1	5729.3	Facies A (Limestone)	−7.97	1.89	1.02
5730.2	YaS1	5730.2	Facies A (Limestone)	−8.43	2.25	1.04
5628.8	XS1	5628.8	Facies B (Dolomite)	−5.84	2.75	0.68
LS1-28	LS1	5987.48	Facies A (Dolomite)	−5.07	2.79	1.42
LS1-53	LS1	5970.82	Facies A (Dolomite)	−6.48	2.19	2.58
LS1-43	LS1	5987.86	Facies A (Dolomite)	−7.39	2.37	0.88
6207.1	YS1	6207.1	Facies C (Dolomite)	−8.49	2.43	4.25
5826.5	PZ1	5826.5	Facies C (Dolomite)	−9.97	2.32	9.27
6219.5	YS1	6219.5	Facies C (Dolomite)	−7.47	2.65	8.14
LS1-31	LS1	5986.08	Facies C (Dolomite)	−7.04	2.41	1.2
LS1-24	LS1	5990.46	Facies C (Dolomite)	−6.02	2.69	1.04
5825.3	PZ1	5825.3	Facies G (Limestone)	−10.33	1.67	1.3
6185.6	YS1	6185.6	Facies G (Dolomite)	−7.95	2.56	1.44
6234.9	YS1	6234.9	Facies G (Dolomite)	−5.77	2.57	5.65
5711.1	XaS1	5711.1	Facies G (Limestone)	−7.02	1.09	1.21

4.4. Diagenesis

4.4.1. Compaction

The mechanical compaction and pressure dissolution (i.e., chemical compaction) were largely developed in T_2l_4, whether in grainstone or microbial carbonates. In grainstone, many intraclasts had a ductile elliptical shape, and a concave–convex contact between particles could be observed. A large number of stylolites, filled with residual asphalt and little pyrite, could be observed (Figure 10a). Obviously, compaction greatly reduced the initial porosity.

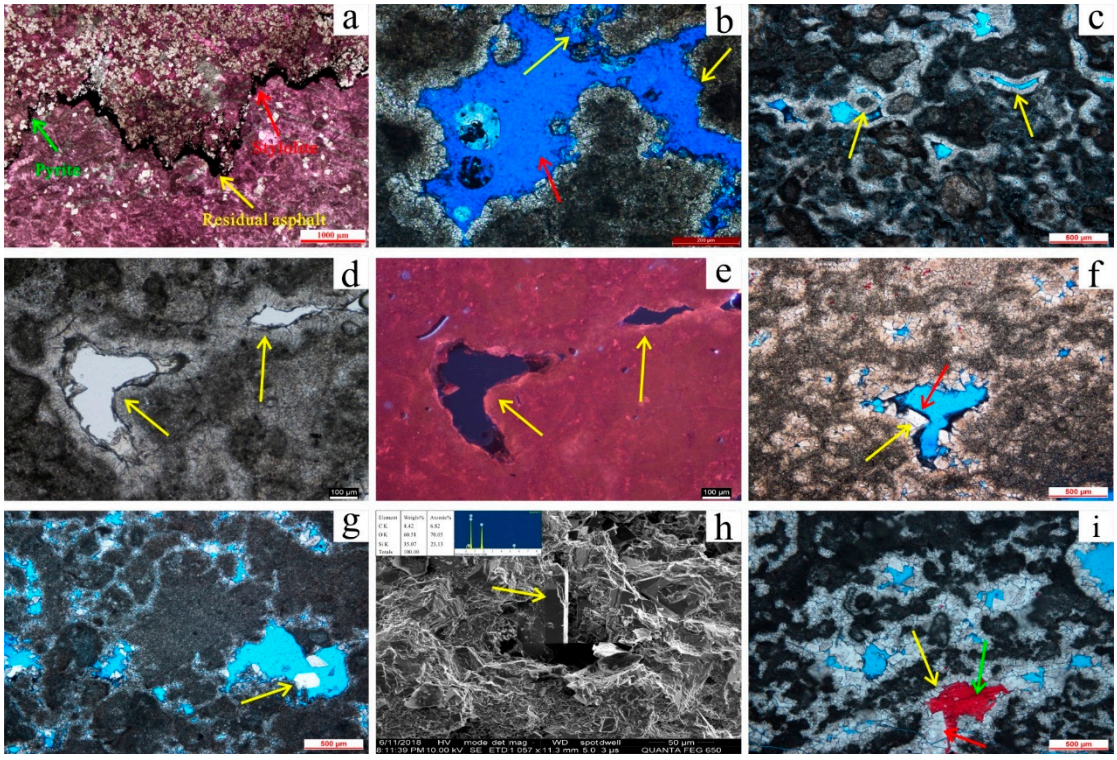

Figure 10. Microscopic characteristics of the diagenesis in the Leikoupo Formation. (**a**) Residual asphalt (yellow arrow) and pyrite (green arrow) in stylolite (red arrow), $T_2l_4^3$, Yangshen-1 well, 6170.51 m; (**b**) Expansion dissolution (yellow arrow) on the basis of early dissolution pores (red arrow), $T_2l_4^3$, Anfu-1 well, 5702.97 m; (**c**) Isopachous and circumgranular dolomite (yellow arrow), $T_2l_4^3$, Yangshen-1 well, 6229.50 m; (**d**) Isopachous and circumgranular dolomite (yellow arrow), $T_2l_4^3$, Yangshen-1 well, 6229.50 m; (**e**) Analysis of isopachous and circumgranular dolomite (yellow arrow) in cathodoluminescence, $T_2l_4^3$, Yangshen-1 well, 6229.50 m; (**f**) Euhedral dolomite (yellow arrow) and residual asphalt (red arrow) around it, $T_2l_4^3$, Yashen-1 well, 5782.60 m; (**g**) Single quartz crystal (yellow arrow), $T_2l_4^3$, Yangshen-1 well, 6229.90 m; (**h**) Single quartz crystal in SEM (yellow arrow), $T_2l_4^3$, Yangshen-1 well, 6229.90 m; (**i**) Dog-tooth dolomite (yellow arrow), euhedral dolomite (red arrow), and calcite (green arrow), $T_2l_4^2$, Yangshen-1 well, 6224.70 m.

4.4.2. Dissolution

In the study area, Lei-4 was mainly subjected to two stages of dissolution. The first stage was the dissolution in the syn-depositional period, which was formed by high-frequency sea-level changes and had the characteristics of fabric selectivity. It was mainly developed in microbial carbonates, which was due to the high terrain of microbial mounds. During the short-term sea-level fall period, the mounds were exposed to meteoric freshwater to undergo leaching, forming a large number of dissolution pores (Figure 4e). The second stage of dissolution was the dissolution during the burial period, which was weaker than that of syn-depositional dissolution and was characterized by expansion dissolution along

the crack or on the basis of early dissolution pores (Figure 10b). The reason for the smaller scale of burial dissolution was that the fluid velocity in the pores was abnormally slow in the deep burial environment. If there is no fracture or hydrothermal influence, the formation water and the surrounding rock are in equilibrium, and the carbonate-formation water reaction was a balancing process under a nearly closed system [63]. In the deep burial system, the equilibrium of the dissolution–precipitation reaction tended in the direction of precipitation as the burial depth increased, which is embodied by a small amount of precipitation of carbonate minerals, while the short-term opening environment (the development of cracks or the injection of acidic fluids) led to a small amount of dissolution of carbonate minerals [64]. Besides, through thermodynamic simulation calculation, after oil and gas charging, the proportion of water–rock in the carbonate reservoir was low, and increasing the porosity of 1% of limestone, with a thickness of 100 m, required 37,000 cubic meters of pore water, while the closed systems did not have sufficient pore water [65,66]. Thus, deep dissolution played an important role in adjusting the early pores in T_2l_4, but its contribution to increasing the reservoir was not significant.

4.4.3. Cementation

Lei-4 experienced multi-stage cementation, which caused reduction of the reservoir quality. After the formation of a microbial framework structure by bonding marl, due to the arid climate and sea level fall, some saline minerals, such as gypsum, precipitated and completely or partially filled between the clots (Figure 4d). Thanks to the syn-depositional dissolution, the gypsum dissolved and pores formed, starting with the precipitate of fibrous high-magnesium calcite around grains. Due to diagenetic alteration, the calcite was dog-tooth, isopachous, and circumgranular (Figure 10c) and was replaced by dolomites later on. Cathodoluminescence analysis showed that the dolomite cement had a dark red light, which was similar to the matrix (Figure 10d,e). This implies that the pore water was probably derived from coeval seawater. Combined with its unique morphology, it indicates that the dolomite cementation occurred in a marine-phreatic environment. As the burial depth increased, the euhedral dolomite crystals slowly precipitated in the pores (Figure 10f). During the medium-deep burial period, the circulation of fluids in the pores was limited. After the precipitate of second-stage dolomite crystals, the third phase of larger dolomite and a small number of quartz crystals precipitated (Figure 10g,h). During the deep burial period, the residual pores was completely filled with clear coarse calcite spar (Figure 10i).

4.4.4. Dolomitization

The dolomite in Lei-4 experienced relatively early dolomitization. The dolomite had an aphanocrystalline to fine crystal size and a dirty surface. The $\delta^{13}C_{VPDB}$ values of limestone ranged from 1.09‰ to 2.25‰ (average 1.73‰), and the $\delta^{13}C_{VPDB}$ values of dolomite ranged from 2.16‰ to 3.75‰ (average 2.56‰), which shows a small difference, so the fluid for dolomitization probably originated from the seawater. In addition, dolomitization preceded the formation of gypsum and anhydrite, which precipitated in the inter-clot pores and fenestral pores. Besides, although it underwent the burial period, it seems that the dolomite was not affected by the relatively strong diagenetic alteration through the analysis of the geochemical data of the whole rock. It lacked the invasion of external fluids, and Machel [30] and Jiang [67] believe that it belongs to the early diagenesis. The evidence presented above indicates that main dolomitization occurred in the relatively early diagenesis stage.

5. Discussion

5.1. Interpretation of Geochemical Characteristics

In general, the LREE of oxidized water was more likely to enter the Mn-Fe oxide or hydroxide than HREE, so the rare earth elements in the oxidized water generally showed a loss of LREE [68,69]. Reductive conditions led to the dissolution of oxides or hydroxide, resulting in the presence of LREE-rich features in weak oxygen and anoxic waters [68,69]. Accordingly, the sedimentary seawaters

of Lei-4 were anoxic. Besides, the REE pattern of different lithofacies in the Leikoupo Formation showed a relatively flat distribution pattern (Figure 9). The reason for this distribution pattern was mainly the participation of microorganisms. In a microbial environment, the carbonate nucleus was more easily formed, and the shape of the crystal was mainly dumbbell-shaped, which is different from chemically precipitated carbonate. These morphological features had an important influence on the entry of elements into the crystal [70], thus affecting the enrichment of rare earth elements. Carbonate rocks (partially microbial stromatolites) of the Precambrian and North China Craton in Eastern China also had a relatively flat distribution pattern of REE [71].

The values of the Ce anomaly were used to determine redox conditions [52,72]. In an oxic environment, Ce^{3+} was oxidized to Ce^{4+} so that the concentration of Ce^{3+} decreased, the negative anomaly of Ce was formed, and the value of the Ce anomaly was less than 1. On the other hand, in an anoxic environment, the concentration of Ce^{3+} increased, the positive anomaly of Ce was formed, and the value of the Ce anomaly was larger than 1 [52,72]. In T_2l_4, MREE is enriched (Figure 8), and the lithofacies G and J sample displayed a slight positive Ce anomaly (varied from 1.010 to 1.052, with an average of 1.024) (Table 4 and Figure 8), which is compelling evidence indicating an anoxic marine environment [73–75]. However, a slight negative Ce anomaly is observed in the microbialites (Facies A, B, and C) samples varied from 0.877 to 1.084 (average 0.962), which indicates an oxic environment of microbialites. The analysis of trace elements makes it clear that the sea water was anoxic. Therefore, we argue that the slightly negative Ce of microbialites is probably due to that the microbialites were exposed to subaerial conditions in the eogenetic period.

In a low-temperature and alkaline environment, Eu^{3+} was reduced to relatively soluble Eu^{2+}, the concentration of Eu^{3+} was decreased, the negative anomaly of Eu occurred, and the value of the Eu anomaly was less than 1. Conversely, in a high-temperature environment, the positive anomaly of Eu was formed, the value of the Eu anomaly was larger than 1, and the significant Eu positive anomaly was mainly affected by hydrothermal fluids [72,76–78]. In T_2l_4, the Eu anomaly varied from 0.559 to 63.876 (average: 8.576, which is much larger than 1) (Table 4 and Figure 8), which indicates that the carbonates in Lei-4 were influenced by hydrothermal fluids in diagenesis, and a small amount of hydrothermal fluorite and sphalerite were also found in the cores [52].

In view of the global Triassic seawater carbon isotope variation curve [79], the biological extinction in the Late Permian led to a reduction of the carbon isotope values (−2‰). In the Triassic, the carbon isotope values began to elevate due to biological recovery during the Annie period (sedimentary period of the Leikoupo Formation), and the carbon isotope value ranged from −1‰ to 2‰. The carbon isotope values of the microbial carbonates in the Leikoupo Formation ranged from 1.09‰ to 3.75‰ (Figure 10), which indicates a positive shifting, compared to the seawater in the same period (Figure 10). There was no coal deposition on the land, so the amount of primitive organic carbon created by terrestrial plants was limited in this period [80]. However, the fixation of CO_2 and the converse of organic carbon to the CO_2 of microbes (e.g., bacteria and algae) could produce a measurable value of $\delta^{13}C$ rising [81]. This has also been proven in the modern marine carbon cycle [82]. Microbes were the first organisms to recover after the Great Extinction, and their photosynthesis reconstructed the isotope fractionation effect of organic carbon destroyed by extinction [80]. Therefore, it is possible that the reason for the positive shift was the large number of microbes in this period.

In the Middle Triassic, the global oxygen isotope values of marine carbonates ranged from −6‰ to −1‰ [79], while the oxygen isotope values of the microbial carbonates in the Leikoupo Formation ranged from −9.97‰ to −3.5‰ (Figure 10), with a negative shift feature. This indicates that the microbial carbonate rocks experienced a meteoric freshwater diagenetic environment in the early stages [83].

5.2. Depositional Environments

5.2.1. Lagoon

Due to the arid climate, the seawater in Anisian was restricted and envaporitic, and the dolomitic lagoon and gypsiferous lagoon stably developed (Figure 11). The dolomitic lagoon was mainly developed in $T_2l_4^3$ and was about 10 to 38 m thick. In the study area, the dolomitic lagoon was dominated by dark gray and microcrystalline to very fine crystalline, and its lithofacies included thrombolites (facies A), bioclastic packstone (facies D) and peloid-dominated packstone to grainstone (facies G). The seawater circulation of the dolomitic lagoon was relatively blocked, so the water energy was weak and miliolinid foraminifera, and few fragments of shells could be found in it. The gypsiferous lagoon developed in $T_2l_4^1$ and $T_2l_4^2$ and was more than 200 m thick. The lithofacies in the gypsiferous lagoon contained anhydrite (facies H), dolomitic anhydrite (facies I), and a small amount of anhydritic thrombolites (facies B), which were dominated by a light white to off-white color and were fine to coarse crystalline (Figure 12).

5.2.2. Microbial Mound

Microbial mounds were mainly developed in the intertidal zone in $T_2l_4^3$ (Figure 11). They were the most widely developed, were about 20 to 48 m thick, and were chiefly composed of thrombolites (facies A) and stromatolites (Facies C) and a small amount of peloid-dominated packstone to grainstone (facies G). The seawater circulation and the hydrodynamic condition were relatively strong, so an undulated laminated microbial structure was dominant. Miliolinid foraminifera and tectulariid foraminifera (single chamber and biserial chamber) were found in the microbial mounds (Figure 12).

5.2.3. Shoal

Shoals were developed in the intertidal zone, with a thickness of about 15 to 38 m (Figure 11). The thickest part was located near the Pengzhou 103 well and had a thickness of 57 m. The lithology combination was dominated by intraclast-dominated grainstone (facies E), microbial clot-dominated grainstone (facies F) and peloid-dominated packstone to grainstone (facies G). Most of the grains were cemented by bright granulous dolomite or calcite, indicating that the hydrodynamic condition was strong, and a small amount of miliolinid foraminifera debris was preserved. The subtidal zone was subdivided into a shallow subtidal subzone and deep subtidal subzone in the study area. The shallow subtidal subzone was dominated by lagoons, while the deep subtidal subzone was less developed in the western margin of the study area, with argillaceous carbonates, dolomicrite, and micrite developed. The deep subtidal subzone was located below the wave base, so the hydrodynamic condition was weak (Figure 12).

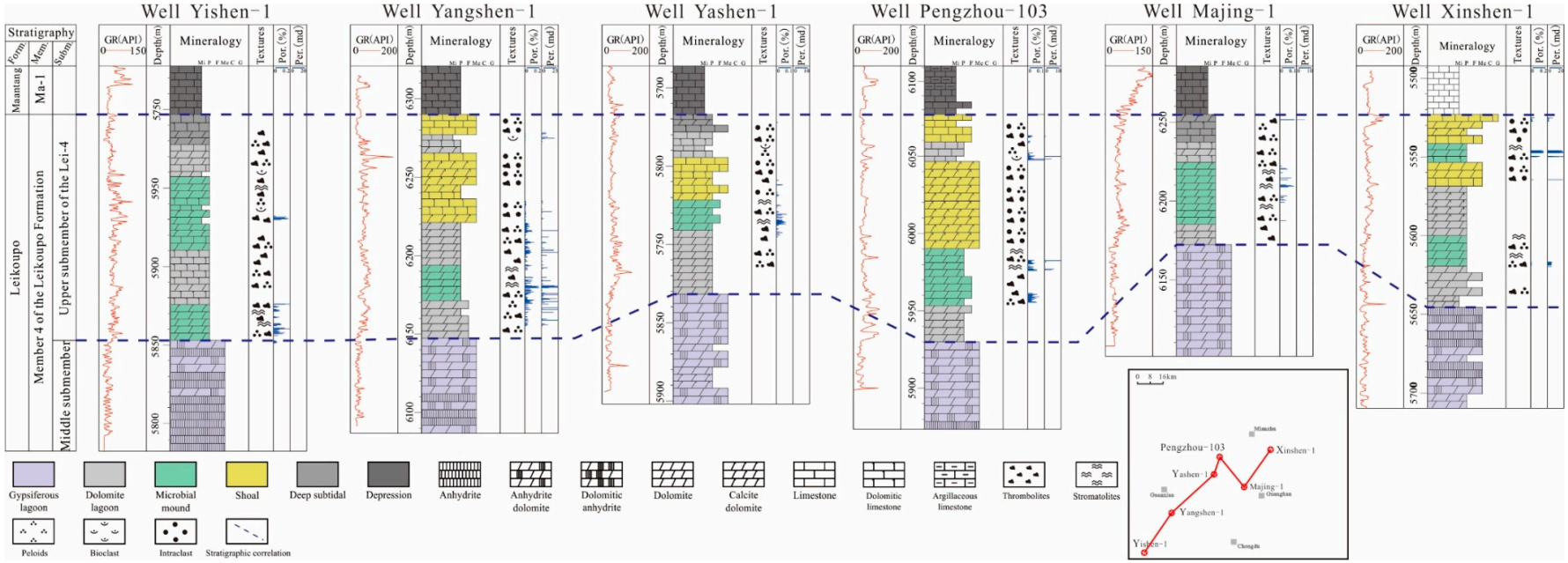

Figure 11. Mineralogy, textures, facies, porosity, and permeability of the middle and upper sub-member of the fourth member of the Leikoupo Formation.

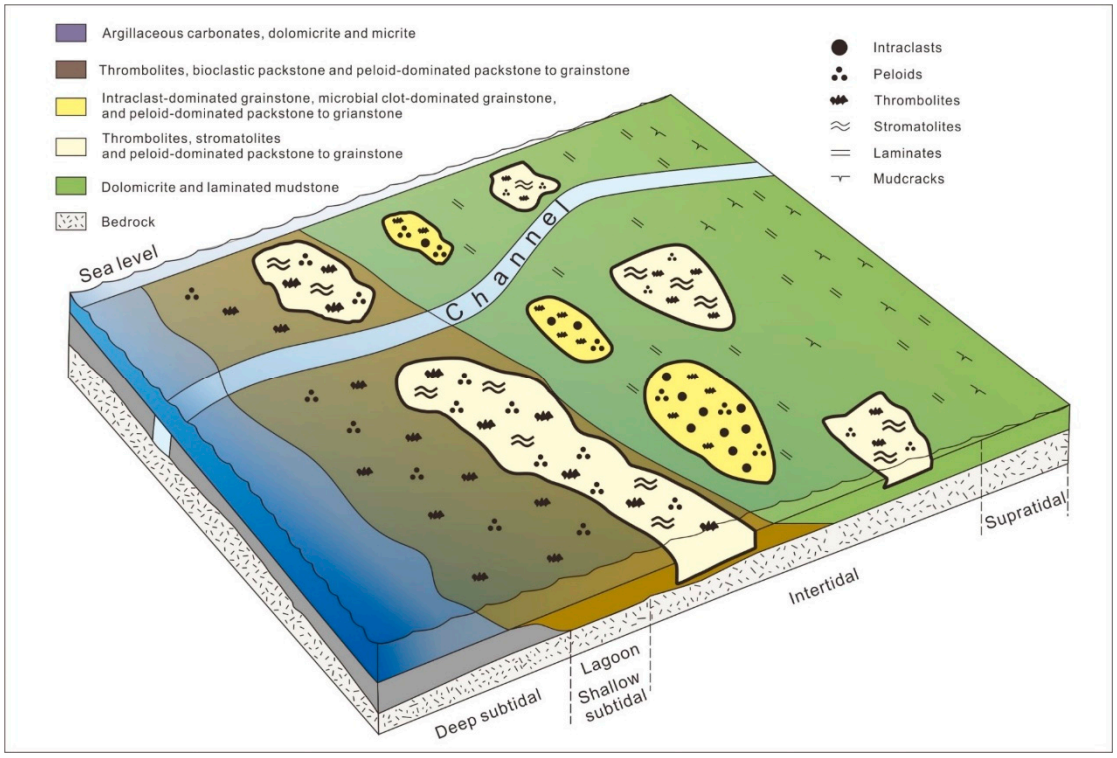

Figure 12. Schematic diagram of the sedimentary environments of the Leikoupo Formation.

5.3. Diagenetic Sequence and Pore Evolution

5.3.1. Eogenetic (Near-Surface) Period

During the eogenetic period, the original calcite marls were captured and bound by microorganisms, the microbial fenestral pores and inter-particle pores were formed, and the seawater was filled in the pores. In the syn-depositional period, extensive dolomitization occurred, and the degree of crystallinity of dolomite crystals was low. The order degree of dolomite was between 0.38 and 0.89 (average 0.64), which was generally low. The early dolomitization could add some pore space due to volume shrinkage, which enhanced the anti-compaction ability of the rocks. Subsequently, the early seawater gradually evaporated and concentrated due to the arid climate, as discussed before, and gypsum gradually precipitated in the microbial fenestral and inter-particle pores. Due to the relative sea-level fall, the gypsum was exposed to the surface and was completely or partially leached by meteoric water. Residual gypsum with an irregular edge could be found in pores. During the relative sea-level rise, the fluid in the pores was converted into seawater, and the fibrous high-magnesium calcite was cemented and subsequently replaced by dolomite. The crystal size of dolomite was very fine to fine. In addition to microbial fenestral pores, intra-particle pores were also developed in this period (Figure 13).

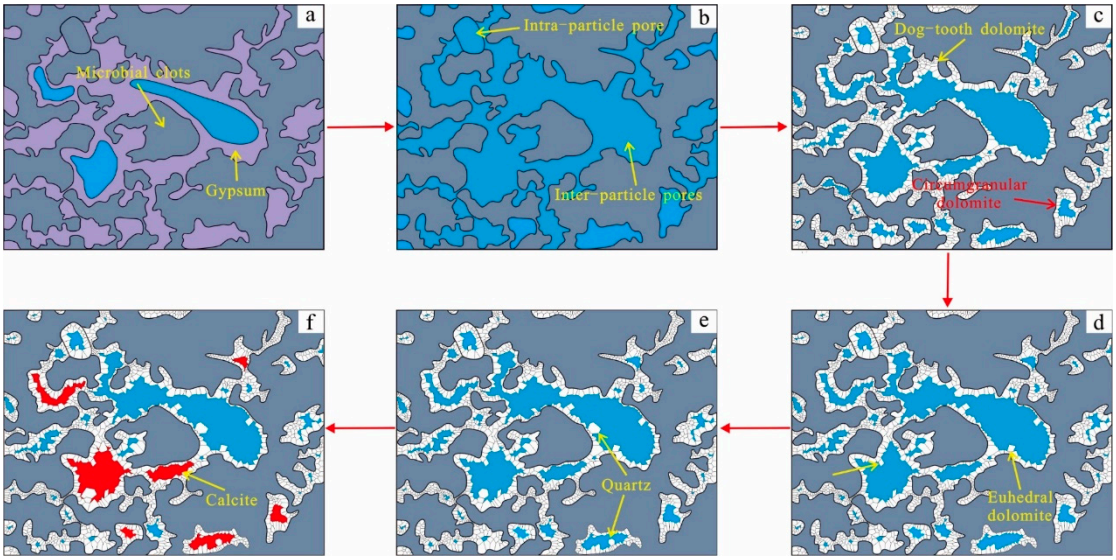

Figure 13. Evolution of microbial inter-particle pores in the Leikoupo Formation. (**a**) In the sedimentary period, initial inter-particle pores formed, and gypsum precipitated from seawater; (**b**) In the syn-depositional period, gypsum and a few clots dissolved, and inter-particle pores and intra-particle pores formed; (**c**) In shallow burial period, circumgranular and dog-tooth cements formed in the pores; (**d**) As the depth increased, euherdral dolomite precipitated; (**e**) Quartz crystal precipitated in the deep burial period; (**f**) Clear coarse calcite spar precipitated in the deep burial period.

5.3.2. Mesogenetic (Burial) Period

During the mesogenetic period, the temperature and pressure increased as the burial depth was increased, and the residual gypsum was dehydrated and converted into anhydrite. In addition, a large number of stylolites were formed. Some of the particles were dissolved, and oil and gas charged during this period. Residual bitumen could be found in the stylolites and around some of the second-stage dolomite crystals. The circulation of the fluid in the pores was limited, and after the second-stage dolomite crystals, the third phase of the larger dolomite and a small amount of single-crystal quartz crystals precipitated. The residual reservoir space in some pores was completely filled by clear coarse calcite during this period, causing damage to the reservoir porosity. Due to the release of stress during the burial process and the influence of structural uplift, three-stage fractures occurred. Acidic or other unsaturated fluids entered the fractures, leading to the occurrence of dissolution, which had a certain positive impact on the reservoir, but the impact was limited due to its low occurrence frequency (Figure 14).

5.4. Impact of Sedimentation and Diagenesis on the Reservoirs of Lei-4

From the tectonic evolution of the western margin of the Yangtze Block, the Middle Triassic belongs to the end stage of the development of the carbonate platform, and the subduction of the western margin of the Yangtze Block to the Songpan Block did not respond to sedimentation. Due to the impact of the subduction, the paleo Tethys Ocean was gradually closed, and the seawater gradually withdrew from the Western Sichuan Basin along the NE-SW direction. The study area was located in the arid climatic zone, and the evolution of life was in the recovery period after the mass extinction. The microorganisms were prosperous in this period.

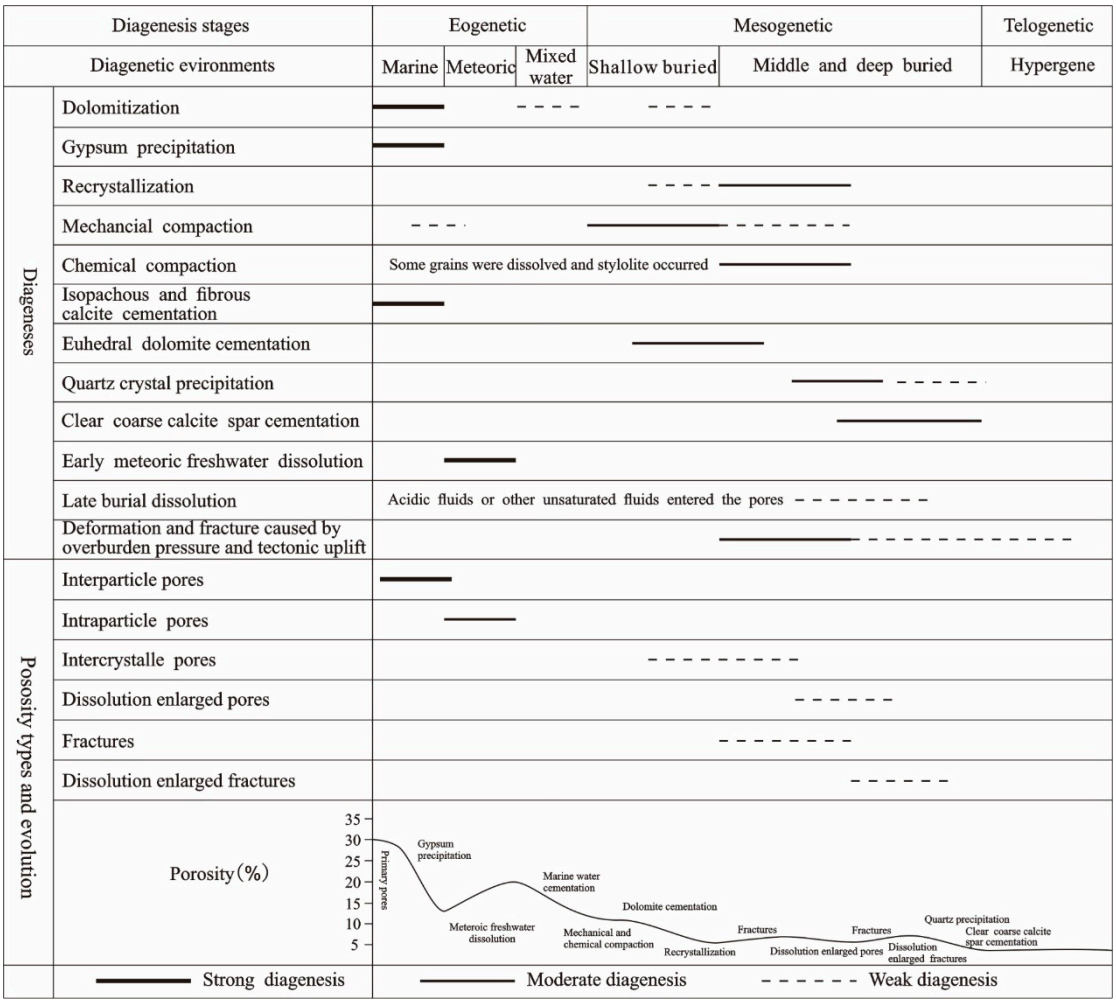

Figure 14. Major diagenesis impacting the reservoir quality of the Leikoupo Formation.

The prosperity of the microorganisms led to the development of microbial carbonate rocks in the Leikoupo Formation, and the microbial mounds were widely distributed in the study area, providing primary pores and a material basis for diagenetic alteration for the development of secondary pores. The behaviors of the microorganisms in capturing marls lacked regularity, resulting in an irregular shape of the clots in the thrombolites. In addition to providing a certain primary pore space, the irregular-shaped clots provided a relatively early anti-compaction skeleton of the primary pores after its consolidation during diagenesis. The microbial mounds had a relatively positive relief, which was conducive to syn-depositional dissolution, laying a foundation for the development of high-quality reservoirs. In addition, from the lateral correlation of the Lei-4 reservoirs, most of the high-quality reservoirs were also developed in the microbial mounds (Figure 11).

The diagenesis affecting the development of microbial carbonate reservoirs in the Leikoupo Formation was mainly early dolomitization and syn-depositional dissolution. Early dolomitization allowed early pores to be effectively preserved. Firstly, in the case of constant porosity, dolomite could create a pore structure (pore size and connectivity) that is better than calcite. Besides, early dolomitization could enhance the rock anti-compaction ability. Early dolomitization could also inhibit compaction during the burial period and was conducive to the preservation of reservoir space. In addition, the syn-depositional dissolution of the gypsum greatly increased the reservoir space.

5.5. Preservation of Pores in Microbial Carbonate Reservoirs

In addition to the preservation of pores by early dolomitization, as mentioned above, the hydrocarbon charging and rapid burial also preserved early pores. Residual bitumen was visible around the second stage of dolomite crystals, which inhibited the further cementation during the burial process (Figure 9f). In addition, from the burial history of the CK-1, GK-1, and PG-1 wells, the Longmen Mountains were rapidly uplifted in the Late Triassic [16,84]. The Xujiahe Formation, the overlying strata of the Leikoupo Formation, deposited great mudstones. The rapid burial caused the Leikoupo Formation to terminate the early near-surface cementation and to create a closed system. The closed system was also conducive to the preservation of early pores. In addition, the thick mudstone in the Xujiahe Formation played a good role in the protection of reservoirs as a high-quality seal.

Micropores is a noteworthy pore type in the Leikoupo Formation for they can contribute to total pore volume, increasing storage capacity for hydrocarbons. The micropores in carbonates with high organic matters, similar to the Leikoupo Formation, originate from the dissolution of organic acid or degradation with the proceeding of the thermal maturation of organic matter in some cases [85,86]. Besides, microbial activity could contribute to the formation of micropores. Micropores that result from the decay of eubacteria are common in travertines [87]. Bosak, Souza-egipsy, Corsetti and Newman [88] found the micropores formed in bacterially-induced calcite. Carbonates in the Leikoupo Formation are typical microbialites which provide the condition for development of micropores. No matter how the micropores formed, the hydrocarbon occluded the micropores could preserved those pores from destructive diagenetic alteration. The occurrence of oil or residual bitumen could indicate the hydrocarbon source and preservation mechanism of micropores [89]. If oil appear as inclusion, this indicates entrapment of oil inclusions after hydrocarbon migration, so the micropores preserved by early oil migration and charging. If oil and bitumen occupy intracrystal pores do not have features of inclusions, which indicates their in situ source, the micropores preserved by maturation of organic matter. However, the data of oil droplets or asphalt within micropores are needed to further explore the preservation of micropores.

6. Conclusions

The Leikoupo Formation in the Western Sichuan Basin of SW China developed microbial carbonate reservoirs. The reservoirs mainly occurred in $T_2l_4^3$, with the main rock types of thrombolites and stromatolites. The pore types were dominated by microbial inter-clot pores, intra-clot pores, and fenestral pores, formed by trapping and binding of marls by benthic microbial communities.

Geochemical analysis shows that the redox condition of the sea water in the period of Lei-4 deposition was anoxic. Both the flat distribution pattern of rare earth elements and the positive drift of carbon isotopes were closely related to microorganisms. The negative drift of oxygen isotope was related to meteoric fresh water, which promoted the formation of early secondary pores.

Microbial carbonate reservoirs in Lei-4 were controlled by sedimentation and diagenesis. Thrombolites and stromatolites are the main high-quality reservoirs rock types developed as microbial mounds. The primary pores, developed in thrombolites and stromatolites, offered the space for diagenetic transformation. The precipitation of gypsum that occurred in synchronous or syn-depositional period was the material basis for the formation of secondary pores. Early dolomitization and syn-depositional dissolution were crucial to the development of the reservoirs.

The four stages of cementation during the burial period destroyed the reservoir to some extent, but the early dolomitization enhanced the anti-compaction ability of microbial carbonates during burial stage. Besides, the hydrocarbon filling after the second stage of cementation inhibited the intrusion of saturated fluid during the subsequent burial period. In addition, rapid burial accelerated the transformation of the reservoirs into a closed system and reduced early cementation.

Author Contributions: Conceptualization, B.L. and Y.W.; methodology, Y.W. and W.J.; software, H.Z. and H.L.; validation, H.L.; formal analysis, Y.W., W.J. and H.L.; investigation, Y.W.; resources, X.S., Q.W., W.W. and Y.L.; data curation, X.S., Q.W., W.W. and Y.L.; writing-original draft preparation, Y.W.; writing-review and editing, B.L., W.J., H.L. and H.Z.; visualization, Y.W., W.J., H.L. and H.Z.; supervision, B.L.; project administration, B.L., X.S., Q.W., W.W. and Y.L.; funding acquisition, B.L., X.S., Q.W., W.W. and Y.L. All authors have read and agreed to the published version of the manuscript.

Funding: The authors would like to thank the National Natural Science Foundation of China (NSFC) and Research Institute of Petroleum Exploration and Development of Southwest Petroleum Branch of SINOPEC. Financial support for the research was provided by NSFC (41572117), Major National Science and Technology Projects, China (2017ZX05005-003-005) and Key Scientific and Technological Project of SINOPEC (P16092).

Conflicts of Interest: The authors declare no conflict of interest.

References

1. Burne, R.V.; Moore, L.S. Microbialites: Organosedimentary deposits of benthic microbial communities. *Palaios* **1987**, *2*, 241–254. [CrossRef]
2. Riding, R. Classification of microbial carbonates. In *Calcareous Algae and Stromatolites*; Springer: Berlin, Germany, 1991; pp. 21–51.
3. Riding, R. Microbial carbonates: The geological record of calcified bacterial-algal mats and biofilms. *Sedimentology* **2000**, *47* (Suppl. 1), 179–214. [CrossRef]
4. Tewari, V.C.; Seckbach, J. *Stromatolites: Interaction of Microbes with Sediments, Cellular Origin, Life In Extreme Habitats and Strobiology*; Springer: Dordrecht, The Netherlands, 2011.
5. Falicia, G. Living stromatolites of Shark Bay, Western Australia: Microbial inhabitants. In *STROMATOLITES: Interaction of Microbes with Sediments, Cellular Origin, Life in Extreme Habitats and Astrobiology*; Tewari, V.C., Seckbach, J., Eds.; Springer: Dordrecht, The Netherlands, 2011; Volume 18, pp. 343–358.
6. Jamie, S.F.; Stefan, J.G. Microbial diversity in modern stromatolites. In *STROMATOLITES: Interaction of Microbes with Sediments, Cellular Origin, Life in Extreme Habitats and Astrobiology*; Tewari, V.C., Seckbach, J., Eds.; Springer: Dordrecht, The Netherlands, 2011; Volume 18, pp. 383–405.
7. Reid, R.P.; Browne, K.M. Interidal stromatolites in a fringing Holocene reef complex, Bahamas. *Geology* **1991**, *19*, 15–18. [CrossRef]
8. Ginsburg, R.N.; Planavsky, N.J. Diversity of Bahamian microbialite substrates. In *Links between Geological Processed, Microbial Activities and Evolution of Life*; Dilek, Y., Furnes, H., Muehlenbachs, K., Eds.; Springer: Dordrecht, The Netherlands, 2008; pp. 177–195.
9. Kathleen, M.B. Modern marine stromatolitic structures: The sediment dilemma. In *STROMATOLITES: Interaction of Microbes with Sediments, Cellular Origin, Life in Extreme Habitats and Astrobiology*; Tewari, V.C., Seckbach, J., Eds.; Springer: Dordrecht, The Netherlands, 2011; Volume 18, pp. 291–312.
10. Maria, E.F.; Daniel, G.P.; Maria, J.A.; Virginia, H.A. Modern stromatolite ecosystems at alkaline and hypersaline high-altitude lakes in the Argentinean Puna. In *STROMATOLITES: Interaction of Microbes with Sediments, Cellular Origin, Life in Extreme Habitats and Astrobiology*; Tewari, V.C., Seckbach, J., Eds.; Springer: Dordrecht, The Netherlands, 2011; Volume 18, pp. 427–441.
11. Santos, F.; Peña, A.; Nogales, B.; Soria, E.; Garcia del Cura, M.A.; González-Martin, J.A.; Antón, J. Bacterial diversity in modern freshwater stromatolites from Ruidera Pools Natural Park, Spain. *Syst. Appl. Microbiol.* **2010**, *33*, 209–221. [CrossRef] [PubMed]
12. Luo, P.; Wang, S.; Li, P.W.; Song, J.M.; Jin, T.F.; Wang, G.Q.; Yang, S.S. Review and prospectives of microbial carbonate reservoirs. *Acta Sedimentol. Sin.* **2013**, *31*, 807–823.
13. Bosence, D.W.J.; Gibbons, K.A.; Heron, D.P.L.; Morgan, W.A. *Microbial Carbonates in Space and Time: Implications for Global Exploration and Production*; Geological Society London Special Publications: London, UK, 2015.
14. Sheehan, P.M.; Harris, M.T. Microbialite resurgence after the Late Ordovician extinction. *Nature* **2004**, *430*, 75–78. [CrossRef] [PubMed]
15. Słowakiewicz, M.; Tucker, M.E.; Pancost, R.D.; Perri, E.; Mawson, M. Upper Permian (Zechstein) microbialites: Supratidal through deep subtidal deposition, source rock, and reservoir potential. *AAPG Bull.* **2013**, *97*, 1921–1936. [CrossRef]

16. Jiang, L.; Worden, R.H.; Cai, C.F.; Shen, A.J.; Crowley, S.F. Diagenesis of an evaporite-related carbonate reservoir in deeply buried Cambrian strata, Tarim Basin, Northwest China. *AAPG Bull.* **2018**, *102*, 77–102. [CrossRef]
17. Baud, A.; Cirilli, S.; Marcoux, J. Biotic response to mass extinction: The lower most Triassic microbialites. *Facies* **1997**, *36*, 238–242.
18. Heydari, E.; Hassanzadeh, J.; Wade, W.J.; Ghazi, A.M. Permian-Triassic boundary interval in the Abadeh section of Iran with implications for mass extinction: Part 1. Sedimentology. *Palaeogeogr. Palaeoclimatol. Palaeoecol.* **2003**, *193*, 405–423. [CrossRef]
19. Hips, K.; Haas, J. Calcimicrobial stromatolites at the Permian-Triassic boundary in a western Tethyan section, Bùkk Mountains, Hungary. *Sediment. Geol.* **2006**, *185*, 239–253. [CrossRef]
20. Wignall, P.B.; Twitchett, R.J. Unusual intraclastic limestones in Lower Triassic carbonates and their bearing on the aftermath of the end-Permian mass extinction. *Sedimentology* **1999**, *46*, 303–316. [CrossRef]
21. Marcoux, J.; Baud, A. The Permo-Triassic boundary in the Antalya nappes (western Taurides, Turkey). *Mem. Soc. Geol. Ital.* **1986**, *34*, 243–252.
22. Liu, S.G.; Song, J.M.; Luo, P.; Qing, H.R.; Lin, T.; Sun, W.; Li, Z.W.; Wang, H.; Peng, H.L.; Yu, Y.Q.; et al. Characteristics of microbial carbonate reservoir and its hydrocarbon exploring outlook in the Sichuan Basin, China. *J. Chengdu Univ. Technol.* **2016**, *43*, 129–152.
23. Zhai, X.F.; Wang, Z.C.; Luo, P.; Wang, T.S.; Shi, S.Y.; Zhang, H. Characteristics and origin of microbial dolomite reservoirs in Upper Sinian Deingying Formation, eastern Gaoshiti area, Sichuan Basin, SW China. *Nat. Gas Geosci.* **2017**, *28*, 1199–1210.
24. Hu, W.X.; Zhu, J.Q.; Wang, X.L.; You, X.L.; He, K. Characteristics, origin and geological implications of the Cambrian microbial dolomite in Keping area, Tarim Basin. *Oil Gas Geol.* **2014**, *35*, 860–869.
25. Li, P.W.; Luo, P.; Song, J.M.; Jin, T.F.; Wang, G.Q. Characteristics and main controlling factors of microbial carbonate reservoirs: A case study of Upper Sinian-Lower Cambrian in the northwestern margin of Tarim Basin. *Acta Pet. Sin.* **2015**, *36*, 1074–1089.
26. Andersen, D.T.; Sumner, D.Y.; Hawes, I.; Webster-Brown, J.; Mckay, C.P. Discovery of large conical stromatolites in Lake Untersee, Antarctica. *Geobiology* **2011**, *9*, 280–293. [CrossRef]
27. Reid, R.P.; Foster, J.S.; Radtke, G.; Golubic, S. Modern Marine Stromatolites of Little Darby Island, Exuma Archipelago, Bahamas: Environmental setting, Accretion Mechanisms and Role of Euendoliths. In *Advances in Stromatolite Geobiology (Lecture Notes in Earth Sciences 131)*; Reitner, J., Quéric, N.V., Arp, G., Eds.; Springer: Berlin, Germany, 2011; pp. 77–89.
28. Allen, M.A.; Goh, F.; Burns, B.P.; Neilan, B.A. Bacterial, archaeal and eukaryotic diversity of smooth and pustular microbial mat communities in the hypersaline lagoon of Shark Bay. *Geobiology* **2009**, *7*, 82–96. [CrossRef]
29. Yu, J.R.; Fan, Z.R. Renqiu buried hill carbonate reservoir research. *Acta Pet. Sin.* **1981**, *2*, 57–70.
30. Mancini, E.A.; Llins, J.C.; Parcell, W.C.; Aurell, M.; Bdenas, B.; Leinfelder, R.R.; Benson, D.J. Upper Jurassic thrombolite reservoir play, northeastern Gulf of Mexico. *AAPG Bull.* **2004**, *88*, 1573–1602. [CrossRef]
31. Grotzinger, J.P.; Amthor, J.E. Facies and Reservoir Architecture of Isolated Microbial Carbonate Platforms, Terminal Proterozoic-Early Cambrian Ara Group, South Oman Salt Basin. *AAPG Annu. Meet.* **2002**, *A67*, 10–13.
32. Wright, P.V.; Racey, A. Pre-salt microbial carbonate reservoirs of the Santos basin, offshore Brazil. In *AAPG Annual Convention and Exhibition*; Al-Ameri, T., Ed.; AAPG: Denver, America, 2009; pp. 7–10.
33. Al Haddad, S.; Mancini, E.A. Reservoir characterization, modeling, and evaluation of Upper Jurassic Smackover microbial carbonate and associated facies in Little Cedar Creek field, southwest Alabama, eastern Gulf coastal plain of the United States. *AAPG Bull.* **2013**, *97*, 2059–2083. [CrossRef]
34. He, D.F.; Ma, Y.S.; Li, Y.Q.; Wu, S.L. New directions in an established gas play: Promising dolomite reservoirs in the Middle Triassic Leikoupo Formation of the Sichuan Basin, China. *AAPG Bull.* **2019**, *103*, 1–29. [CrossRef]
35. Song, X.B.; Wang, Q.X.; Long, K.; Xu, G.M.; Shi, G.S.; Feng, X.; Deng, Q.; Cai, Z.H. Characteristics and main controlling factors of middle Triassic Leikoupo paleokarst reservoirs in Western Sichuan Basin. *Mar. Orig. Pet. Geol.* **2013**, *18*, 8–14.
36. Xu, G.M.; Song, X.B.; Feng, X.; Long, K.; Wang, Q.X.; Shi, G.S.; Zhu, L. Gas potential of the Middle Triassic Leikoupo Fm in the Western Sichuan Basin. *Nat. Gas Ind.* **2013**, *33*, 8–14.

37. Wu, S.X.; Li, H.T.; Long, S.X.; Liu, Z.L.; Wang, C.L.; Zhang, J.T. A study on characteristics and diagenesis of carbonate reservoirs in the Middle Triassic Leikoupo Formation in western Sichuan Depression. *Oil Gas Geol.* **2011**, *32*, 542–559.
38. Li, R.; Long, K.; Song, X.B.; Xu, G.M.; Wang, Q.X.; Wang, D. Characteristics of high frequency sequence and control factors of development of the third bed of the member 4 of Leikoupo Formation in Western Sichuan Basin, China. *J. Chengdu Univ. Technol.* **2016**, *43*, 582–590. [CrossRef]
39. Wang, H. The Characteristics and Main Controlling Factors of the Fourth Member of Middle Triassic Leikoupo Formation Microbialite Reservoir in the Western Sichuan Basin. Master's Thesis, Chengdu University of Technology, Chengdu, China, 2018; pp. 1–146.
40. Li, H.T.; Hu, X.Y.; Shi, Y.Q.; Xiao, K.H.; Jia, Y.W.; Wei, X.P.; Feng, Q. Sequence division and controlling factors of reservoir development of the 4th Member of Leikoupo Formation in foreland of Longmen Mountains in the Western Sichuan Depression, Sichuan Basin. *Oil Gas Geol.* **2017**, *38*, 753–763.
41. Wang, Q.X.; Song, X.B.; Wang, D.; Long, K. Reservoir characteristics and formation mechanism of the 4th member of the Leikoupo Formation in Longmen Mountain front. *Pet. Geol. Exp.* **2017**, *39*, 491–497.
42. He, D.F.; Li, D.S.; Zhang, G.W.; Zhao, L.Z.; Fan, C.; Lu, R.Q.; Wen, Z. Formation and evolution of multi-cycle superposed Sichuan Basin, China. *Chin. J. Geol.* **2011**, *46*, 589–606.
43. Li, J.H.; Wang, H.H.; Li, W.B.; Zhou, X.B. Discussion on global tectonics evolution from plate reconstruction in Phanerozoic. *Acta Pet. Sin.* **2014**, *35*, 207–218.
44. Liu, H.F.; Liang, H.S.; Cai, L.G.; Shen, F. Structural styles of the Longmenshan thrust belt and evolution of the foreland basin in western Sichuan Provence, China. *Acta Geol. Sin.* **1994**, *7*, 351–372.
45. Liu, S.G.; Sun, W.; Zhong, Y.; Deng, B.; Song, J.M.; Ran, B.; Luo, Z.L.; Han, K.Y. Evolutionary episodes and their characteristics within the Sichuan marine craton basin during Phanerozoic Eon, China. *Acta Petrol. Sin.* **2017**, *33*, 1058–1072.
46. Wu, Y.L.; Yan, Y.J.; Qin, J.H. Palaeogeographic reconstruction of the western margin of the Yangtze platform during the Early and Middle Triassic. *Sediment. Geol. Tethyan Geol.* **1995**, *15*, 17–33.
47. Meng, Q.R.; Zhang, G.W. Timing of collision of the north and south China blocks: Controversy and reconciliation. *Geology* **1999**, *27*, 123–126. [CrossRef]
48. Li, S.B.; Xu, G.M.; Song, X.B. Forming conditions of Pengzhou large gas field of Leikoupo Formation in Longmenshan piedmont tectonic belt, Western Sichuan Basin. *China Petroleum Exploration.* **2016**, *21*, 74–82.
49. Tang, Y. Characterization of the sedimentation of the Leikoupo Formation and the weathering crust reservoirs at the top of the formation in the Western Sichuan Basin. *Oil Gas Geol.* **2013**, *34*, 42–47.
50. Li, L.; Tan, X.C.; Cao, J.; Zou, C.; Ding, X.; Yang, G.; Ying, D.L. Origins of evaporites in the Middle Triassic Leikoupo Formation of the Sichuan Basin, southwest China and their geological implications. *Carbonates Evaporites* **2014**, *29*, 55–63. [CrossRef]
51. Wang, W.K.; Xu, G.M.; Song, X.B.; Long, K.; Chen, Y. Genesis of gypsum-salt in the Leikoupo Formation and its hydrocarbon significance in the Sichuan Basin, China. *J. Chengdu Univ. Technol.* **2017**, *44*, 697–707.
52. Liang, S.Y.; Chen, Y.B.; Zhao, G.W.; Wang, Y.Q.; Hu, Y. Geochemical characteristics of rare earth elements and their geological significance in the fourth member of the Middle Triassic Leikoupo Formation in Western Sichuan Basin. *Pet. Geol. Exp.* **2017**, *39*, 94–98.
53. Chen, J.Y.; Han, Z.Z.; Fan, H.H.; Chi, N.J. Characteristics and Formation Mechanism of Cambrian Thrombolite in Western Shandong Province. *Acta Geol. Sin.* **2014**, *88*, 967–979.
54. Moore, C.H. *Carbonate Reservoirs-Porosity Evolution and Diagenesis in a Sequence Stratigraphy Framework. Elsevier Science*; Elsevier: Amsterdam, The Netherlands, 2001.
55. Brand, U.; Veizer, J. Chemical diagenesis of multicomponent carbonate system-2: Trace elements. *J. Sediment Petrol.* **1980**, *50*, 1219–1236.
56. Huang, S.J. Cathodoluminescence and diagenetic alteration of marine carbonate minerals. *Sediment. Facies Palaeogeogr.* **1990**, *10*, 9–15.
57. Kaufman, A.J.; Knoll, A.H. Neoproterozoic variations in the C-isotopic composition of seawater: Stratigraphic and biogeochemical implications. *Precambrian Res.* **1995**, *73*, 27–49. [CrossRef]
58. Kaufman, A.J.; Jacobsen, S.B.; Knoll, A.H. The Vendian record of Sr and C isotopic variations in seawater: Implications for tectonics and paleoclimate. *Earth Planet. Sci. Lett.* **1993**, *120*, 409–430. [CrossRef]

59. Jiang, Q.C.; Ma, Y.S.; Shen, Y.C.; Guo, R.T.; Gao, X.Q.; Liu, B.; Cui, J.; Wu, K.Y. High-frequency redox variations of the Eocene cyclic lacustrine sediments in the Yingxi area, western Qaidam Basin, China. *J. Asian Earth Sci.* **2019**, *174*, 135–151. [CrossRef]
60. Hatch, J.R.; Leventhal, J.S. Relationship between inferred redox potential of the depositional environment and geochemistry of the Upper Pennsylvanian (Missourian) stark shale member of the Dennis Limestone, Wabaunsee County, Kansas, USA. *Chem. Geol.* **1992**, *99*, 65–82. [CrossRef]
61. Jones, B.; Manning, D.A.C. Comparison of geochemical indices used for the interpretation of palaeoredox conditions in ancient mudstones. *Chem. Geol.* **1994**, *111*, 111–129. [CrossRef]
62. Rimmer, S.M. Geochemical paleoredox indicators in Devonian-Mississippian black shales, Central Appalachian Basin (USA). *Chem. Geol.* **2004**, *206*, 373–391. [CrossRef]
63. Bjørlykke, K.; Jahren, J. Open closed geochemical systems during diagenesis in sedimentary basins: Constraints on mass transfer during diagenesis and the prediction of porosity in sandstone and carbonate reservoirs. *AAPG Bull.* **2012**, *96*, 2193–2214. [CrossRef]
64. Zhang, S.M.; Liu, B.; Qin, S.; Tian, Y.J.; Zhang, X.F.; Guo, R.T. Deeply buried diagenetic process and its significance for the carbonate of Changxing Formation in the northeastern Sichuan Basin. *Acta Petrol. Sin.* **2017**, *33*, 1295–1304.
65. Ehrenberg, S.N.; Walderhaug, O.; Bjørlykke, K. Carbonate porosity creation by mesogenetic dissolution: Reality or Illusion? *AAPG Bull.* **2012**, *97*, 345. [CrossRef]
66. Hao, F.; Zhang, X.F.; Wang, C.W.; Li, P.P.; Guo, T.L.; Zou, H.Y.; Zhu, Y.M.; Liu, J.Z.; Cai, Z.X. The fate of CO_2, derived from thermochemical sulfate reduction (TSR) and effect of TSR on carbonate porosity and permeability, Sichuan Basin, China. *Earth-Sci. Rev.* **2015**, *141*, 154–177. [CrossRef]
67. Jiang, L.; Cai, C.F.; Worden, R.H.; Crowley, S.F.; Jia, L.Q.; Zhang, K.; Duncan, L. Multiphase dolomitization of deeply buried Cambrian petroleum reservoirs, Tarim Basin, north-west China. *Sedimentology* **2016**, *63*, 2130–2157. [CrossRef]
68. Bau, M.; Möller, P.; Dulski, P. Yttrium and lanthanides in eastern Mediterranean seawater and their fractionation during redox-cycling. *Mar. Chem.* **1997**, *56*, 123–131. [CrossRef]
69. Zhao, Y.Y.; Li, S.Z.; Li, D.; Guo, L.L.; Dai, L.M.; Tao, J.L. Rare Earth Element Geochemistry of Carbonate and its Paleoenvironmental Implications. *Geotecton. Metallog.* **2019**, *43*, 141–167.
70. Paquette, J.; Reeder, R.J. Relationship between surface structure, growth mechanism, and trace element in corporation in calcite. *Geochim. Cosmochim. Acta* **1995**, *59*, 735–749. [CrossRef]
71. Liu, Q.Q.; Chi, Q.H.; Wang, X.Q.; Zhou, J.; Liu, H.L.; Liu, D.S.; Gao, Y.F.; Zhai, D.X. Distribution and influencing factors of rare earth elements in carbonate rocks along three continental-scale transects in eastern China. *Earth Sci. Front.* **2018**, *25*, 99–115.
72. Hu, Z.G.; Zheng, R.C.; Hu, J.Z.; Wen, H.G.; Li, Y.; Wen, Q.B.; Xu, F.B. Geochemical characteristics of rare earth elements of Huanglong Formation dolomites reservoirs in Eastern Sichuan—Northern Chongqing area. *Acta Geol. Sin.* **2009**, *83*, 782–790.
73. Bau, M. Rare earth element mobility during hydrothermal and metamorphic fluid-rock interaction and the significance of the oxidation state of europium. *Chem. Geol.* **1991**, *93*, 219–230. [CrossRef]
74. Bau, M.; Koschinsky, A. Oxidative scavenging of cerium on hydrous Fe oxide: Evidence from the distribution of rare earth elements and yttrium between Fe oxides and Mn oxides in hydrogenetic ferromanganese crusts. *Geochem. J.* **2009**, *43*, 37–47. [CrossRef]
75. Banerjee, A.; Słowakiewicz, M.; Majumder, T.; Sayani, K.; Sarbani, P.; Maurice, E.T.; Dilip, S. A Palaeoproterozoic dolomite (Vempalle Formation, Cuddapah Basin, India) showing Phanerozoic-type dolomitisation. *Precambrian Res.* **2019**, *328*, 9–26. [CrossRef]
76. Kamber, B.S.; Webb, G.E. The geochemistry of late Archaean microbial carbonate: Implications for ocean chemistry and continental erosion history. *Geochim. Cosmochim. Acta* **2001**, *65*, 2509–2525. [CrossRef]
77. Van Kranendonk, M.J.; Webb, G.E.; Kamber, B.S. Geological and trace element evidence for a marine sedimentary environment of deposition and biogenicity of 3.45 Ga stromatolitic carbonates in the Pilbara Craton, and support for a reducing Archaean ocean. *Geobiology* **2003**, *1*, 91–108. [CrossRef]
78. Franchi, F.; Hofmann, A.; Cavalazzi, B.; Wilson, A.; Barbieri, R. Differentiating marine vs hydrothermal processes in Devonian carbonate mounds using rare earth elements (Kess mounds, Anti-Atlas, Morocco). *Chem. Geol.* **2015**, *409*, 69–86. [CrossRef]

79. Korte, C.; Kozur, H.W.; Veizer, J. δ13C and δ18O values of Triassic brachiopods and carbonate rocks as proxies for coeval seawater and palaeotemperature. *Palaeogeogr. Palaeoclimatol. Palaeoecol.* **2005**, *226*, 287–306. [CrossRef]
80. Huang, S.J.; Huang, K.K.; Lü, J.; Lan, Y.F. Carbon isotopic composition of Early Triassic marine carbonates, Eastern Sichuan Basin, China. *Sci. China Earth Sci.* **2012**, *55*, 2026–2038. [CrossRef]
81. Sumner, D.Y. Microbial Influences on Local Carbon Isotopic Ratios and Their Preservation in Carbonate. *Astrobiology* **2001**, *1*, 57–70. [CrossRef]
82. Kolber, Z.S.; Plumley, F.G.; Lang, A.S.; Beatty, J.T.; Blankenship, R.E.; VanDover, C.L.; Vetriani, C.; Koblizek, M.; Rathgeber, C.; Falkowski, P.G. Contribution of aerobic photoheterotrophic bacteria to the carbon cycle in the ocean. *Science* **2001**, *292*, 2492–2495. [CrossRef] [PubMed]
83. Chen, R.K. Application of Stable Oxygen and Carbon Isotope in the Research of Carbonate Diagenetic Environment. *Acta Sedimentol. Sin.* **1994**, *12*, 11–21.
84. Qiu, N.S.; Qin, J.Z.; McInnes, B.; Wang, J.; Teng, G.E.; Zheng, L.J. Tectonothermal evolution of the northeastern Sichuan Basin: Constraints from apatite and zircon (U-Th)/He ages and vitrinite reflectance data. *Geol. J. China Univ.* **2008**, *14*, 223–230.
85. Zhao, X.; Qing, L.; Jiang, Z.; Zhang, R. Organic geochemistry and reservoir characterization of the organic matter-rich calcilutite in the Shulu Sag, Bohai Bay Basin, North China. *Mar. Pet. Geol.* **2014**, *51*, 239–255. [CrossRef]
86. Słowakiewicz, M.; Mikołajewski, Z. Sequence stratigraphy of the Upper Permian Zechstein Main Dolomite carbonates in western Poland: A new approach. *J. Pet. Geol.* **2009**, *32*, 215–234. [CrossRef]
87. Chafetz, H.S. Porosity in bacterially induced carbonates: Focus on micropores. *AAPG Bull.* **2013**, *97*, 2103–2111. [CrossRef]
88. Bosak, T.; Souza-egipsy, V.; Corsetti, F.A.; Newman, D.K. Micrometer-scale porosity as a biosignature in carbonate crusts. *Geology* **2004**, *32*, 781–784. [CrossRef]
89. Słowakiewicz, M.; Perri, E.; Tucker, M.E. Micro- and nanopores in tight Zechstein 2 carbonate facies from the Southern Permian Basin, NW Europe. *J. Pet. Geol.* **2016**, *39*, 149–168. [CrossRef]